Constant Mean Curvature Surfaces from Discrete Harmonic Maps

YOUSUF SOLIMAN, Side Effects Software, Canada
PETER SCHRÖDER, University of Bonn, Germany and Caltech, USA
ULRICH PINKALL, TU Berlin, Germany

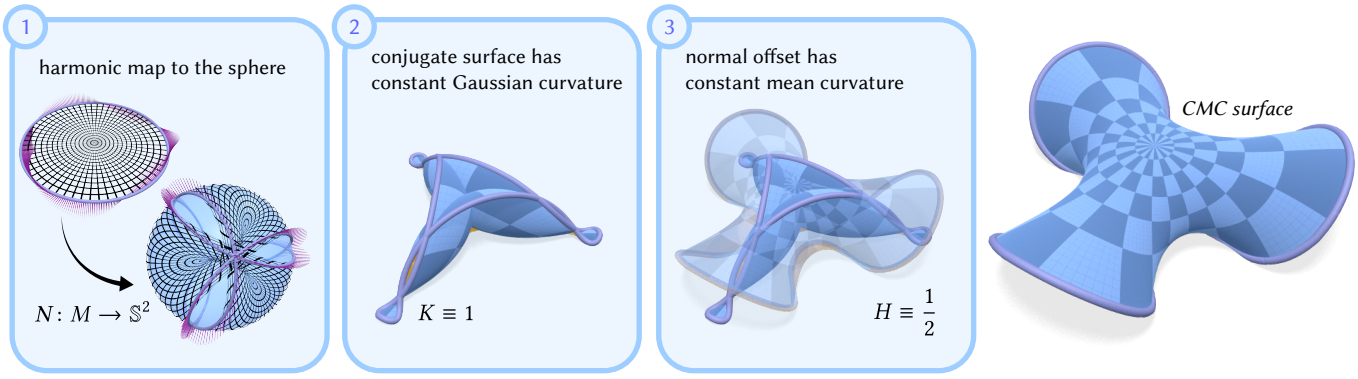

Fig. 1. **Constant Mean Curvature from Normals.** The variations of the normal vectors of a surface in $\mathbb{R}^3$ encode geometric quantities like Gauß and mean curvature. When these normal vectors are harmonic, the resulting surface has constant mean curvature. Our discretization of CMC surfaces is based on this characterization, and it can be used to efficiently solve the free boundary problem with tangent planes specified along the boundary. Starting from a discrete harmonic map (*left*) we construct a discrete conjugate surface (*middle*) by solving a Poisson equation and obtain discrete CMC surfaces as unit normal offsets (*right*).

Constant mean curvature surfaces are æsthetically appealing geometric objects with applications in physics, differential geometry, and architecture. We present a straightforward discretization of constant mean curvature surfaces based on the classical observation that their Gauß maps are harmonic. Our construction is elementary—requiring only discrete Dirichlet energy minimization and a Poisson solve—yet it exactly mirrors this aspect of the smooth theory. A discrete analog of conjugation produces discrete constant Gauß curvature surfaces. Their unit offsets are discrete CMC surfaces with a conformal parameterization. Additionally, we introduce a novel Möbius-invariant discretization of the Dirichlet energy for sphere-valued maps on dual meshes that is derived from the discrete Willmore energy. It is more robust than standard formulations based on inverse cotangent weights. Our approach to the construction of constant mean curvature surfaces provides direct control over tangent planes along a boundary, if present, and naturally handles closed and periodic examples. We demonstrate the approach on a range of free-boundary, symmetric, and periodic CMC surfaces.

CCS Concepts: • **Computing methodologies** → **Shape modeling**; • **Mathematics of computing** → *Partial differential equations*; *Discretization.*

ACM Reference Format:
Yousuf Soliman, Peter Schröder, and Ulrich Pinkall. 2026. Constant Mean Curvature Surfaces from Discrete Harmonic Maps. *ACM Trans. Graph.* 45, 4, Article 143 (July 2026), 16 pages. https://doi.org/10.1145/3811370

Authors' Contact Information: Yousuf Soliman, Side Effects Software, Canada; Peter Schröder, University of Bonn, Germany and Caltech, USA; Ulrich Pinkall, TU Berlin, Germany.

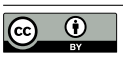

ACM 1557-7368/2026/7-ART143
https://doi.org/10.1145/3811370

1 Introduction

Constant mean curvature (CMC) surfaces model shapes ranging from elastic membranes [Plateau 1873; Otto 1967] to architectural forms [Otto and Rasch 1995; Tellier et al. 2018; Pellis et al. 2020] and are of interest due to their æsthetic as well as structural properties. Mathematically, a surface has constant mean curvature H if the average of its principal curvatures equals H at every point. We refer to such surfaces as CMC-H surfaces. While minimal, *i.e.*, CMC-0 surfaces are the most well-studied, applied, and computationally accessible examples of constant mean curvature surfaces [Pinkall and Polthier 1993; Wang and Chern 2021], their general ($H \neq 0$) construction, discretization, and design continue to be studied.

Techniques for computing discrete CMC surfaces generally fall into two categories: volume constrained area minimization on triangle meshes [Brakke 1992; Pan et al. 2012], and explicit constructions using discrete integrable systems [Hoffmann 1999; Bobenko et al. 2024]. Both strategies discretize different aspects of the smooth theory. We instead discretize the classical relationship between CMC surfaces and harmonic maps into the 2-sphere. The result is a straightforward construction that mirrors the smooth theory.

Similar to the Weierstraß representation [Weierstraß 1866] of minimal surfaces, which generates a CMC-0 surface from a holomorphic map into $\mathbb{S}^2$, the geometry of a CMC-H surface, $H \neq 0$, can be constructed from an arbitrary *harmonic* map into $\mathbb{S}^2$ [Hélein 2001]. In the smooth setting, the construction is achieved by first computing a generalized conjugate of the Gauß map, which yields a surface of constant Gauß curvature in $\mathbb{R}^3$. By a result due to Bonnet [1853] the parallel offsets of this conjugate surface produce a

pair of CMC surfaces. Our approach is a discretization of this theory, providing a simple and straightforward method for modeling CMC surfaces with triangle meshes. A unique feature of our approach is that our variables are the surface normals rather than positions. Hence specifying Dirichlet boundary conditions on the Gauß map produces free boundary CMC surfaces with prescribed tangent planes along the boundary.

Representing CMC surfaces through their Gauß map offers new perspectives on shape modeling. The Gauß map is scale-invariant—it encodes shape but not size—making this representation natural for design workflows where form is developed first. This representation also enables a new optimal approximation problem, finding the CMC surface whose Gauß map best matches that of a given input (Figure 10). Moreover, Dirichlet energy minimization can construct CMC surfaces that are inaccessible to volume-constrained area minimization, including visually striking symmetric and periodic examples which are of independent interest in mathematics. Notably our approach is conformal, facilitating direct transfer of textures and patterns from the design domain.

Contributions. We present a straightforward algorithm for the construction of discrete CMC surfaces, controlling surfaces through their Gauß map. Our main contributions are:

- a structure-preserving discretization of conformal CMC surfaces based on a harmonic map into $\mathbb{S}^2$—requiring only Dirichlet energy minimization;
- a Möbius geometric discretization of the Dirichlet energy for $\mathbb{S}^2$-valued maps on the dual mesh that is more robust than formulations based on inverse cotangent weights;
- demonstration that tangent plane boundary conditions provide an effective interface for designing free-boundary, symmetric, and periodic CMC surfaces.

1.1 Related Work

The discretization and computation of surfaces with distinguished curvature properties has a long history in computer graphics and mathematics, and the study of these surfaces continues to attract investigation.

Discrete Approaches to Constant Mean Curvature. Numerous theories of discrete CMC surfaces have been presented and arise from discretizations of equivalent, but distinct, characterizations of the mean curvature in smooth differential geometry. We review the discrete theories most closely related to ours, along with algorithms for their computation that have been proposed in the literature. The most direct approach to discretizing CMC surfaces is through discretization of their variational characterization as volume-constrained critical points of the area functional as done by Polthier and Rossman [2002]. Several methods compute these discrete CMC surfaces by minimizing a weighted linear combination of the mesh area and enclosed volume including the *SurfaceEvolver* of Brakke [1992]. Replacing the area by the Dirichlet energy, Dziuk and Hutchinson [2006] produce FEM approximations of conformally parameterized CMC disks. This method minimizes a linear combination of the Dirichlet energy and the enclosed volume with a free boundary condition that requires the consideration of reparameterizations of the boundary

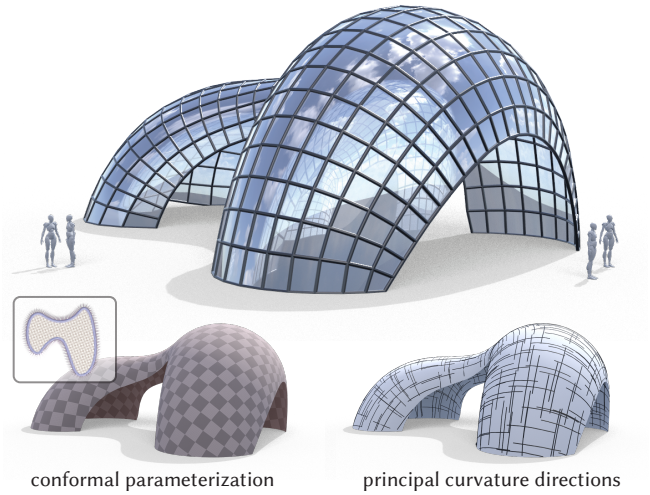

Fig. 2. **Architectural CMC Forms.** A free-boundary CMC surface with tangent planes agreeing with the binormals of a planar domain. The result is a conformally parameterized inflated architectural form that we envision as a glass and steel curvature-aligned gridshell structure. The principal stress directions align with the principal curvature directions, and due to the harmonicity of the Gauß map, the surface exhibits good visual smoothness.

curve. As is typical when simulating a variety of geometric flows, the direct minimization of area (or related energies) exhibits degenerating mesh quality, which Pan et al. [2012] address by including a centroidal Voronoi tesselation energy along with a remeshing step to robustly compute these surfaces. Another class of variational methods minimize an energy subject to a constraint on the discrete mean curvature directly [Smith 2003]; this approach can also be realized using the *ShapeUp* algorithm of Bouaziz et al. [2012]. Since CMC surfaces are also constrained Willmore surfaces [Soliman et al. 2021], they can also be computed using the conformal Willmore flow when the domain is a topological disk [Crane 2013]. Their approach shares some similarities with ours as it also produces a conformally parameterized surface, though it treats the mean curvature as the fundamental variable, is restricted to disk topologies, and exposes control over the boundary binormals instead of the tangent planes.

Discrete CMC surfaces are also closely related to integrable systems in discrete differential geometry. Oberknapp and Polthier [1997] use a discrete version of Lawson's correspondence to transform the problem of computing CMC surfaces into the simpler problem of computing minimal surfaces in $\mathbb{S}^3$. As with our method, their discrete algorithm can also be understood as a discrete conjugation algorithm in the same spirit as the conjugation of discrete minimal surfaces introduced by Pinkall and Polthier [1993] for minimal surfaces in $\mathbb{R}^3$. However, the relationship between the geometry of a CMC surface and its corresponding minimal surface in $\mathbb{S}^3$ is much less direct than the relationship to its Gauß map—this proves to be a fundamental challenge to using this technique for developing an intuitive interface for modeling CMC surfaces. The newly developed theory of discrete CMC surfaces in terms of ring patterns by Bobenko et al. [2024] also reconstructs the surface from

a discretization of the Gauß map (Theorem 6.1), but the role of the Gauß map is played by a $\mathbb{S}^2$ Koebe net. The discretizations of surfaces with constant negative Gauß curvature introduced and studied by Bobenko and Pinkall [1996] is one of the foundational works in the field of discrete integrable systems and is also related to our discretization of surfaces with constant positive Gauß curvature. In both cases, these discrete K-surfaces are characterized in terms of discrete harmonicity of their Gauß map (in $\mathbb{R}^{2,1}$ and $\mathbb{S}^2$, respectively).

Architectural Geometry. Organic freeform surfaces with distinguished curvature properties play an increasingly prominent role in contemporary architecture due to their favorable structural properties and simplified fabrication [Tellier et al. 2018, 2023]. CMC surfaces, in particular, are well-suited to supporting a uniform normal load, typically present in an inflatable structure, since in this case the principal stresses are equal and constant; hence, the stress tensor is a constant multiple of the identity [Rogers and Schief 2003, Equations 3.5 and 3.6]. Since all directions are principal stress directions the fabrication of a CMC surface as a gridshell is optimal. CMC surfaces are also special examples of (linear) Weingarten surfaces, which, when discretized with N panels, can be approximated well using $\sqrt{N}$ molds [Pellis et al. 2021]. They also carry an orthogonal network of curves of constant normal curvature (the angle bisectors of the principal curvature directions), and can therefore be constructed as grid shells from circular strips with a fixed radius [Schling 2018; Pellis et al. 2020].

Discrete Dirichlet Energies. Discretizations of the Laplace-Beltrami operator and the Dirichlet energy for scalar functions have been extensively studied with the aim to maintain a multitude of properties from the smooth setting: *e.g.*, that it is negative semi-definite, symmetric, and maintains linear precision. The cotangent Laplacian on triangulated surfaces satisfies all of these properties when the triangulation is intrinsically Delaunay [Wardetzky et al. 2007]. Discretizations of the Dirichlet energy for more general polygonal meshes are also widely used based on virtual refinement [Bunge et al. 2020] or projection of the polygons onto a best fitting plane [Alexa and Wardetzky 2011]. These discretizations can also be used to measure the Dirichlet energy of sphere valued maps since $\mathbb{S}^2 \subset \mathbb{R}^3$; though in this specialized context, which is only what is needed to define harmonicity of the Gauß map, further refinements to the discretizations have also been considered. Friedel et al. [2007] locally rescale the edge weights so that the discretization approximates the Dirichlet energy of $\mathbb{S}^2$-valued maps from above—this enables the robust computation of unconstrained spherical parameterizations. Discrete bending energies [Bridson et al. 2003; Grinspun et al. 2003; Bobenko 2005] also give rise to discretizations of the Dirichlet energy of the face normals; these bending energies can be expressed in terms of the dihedral angle and intrinsic geometric quantities [Tamstorf and Grinspun 2013] and therefore can be used to define discretizations of the Dirichlet energy for $\mathbb{S}^2$-valued maps defined on the dual of a triangulated surface.

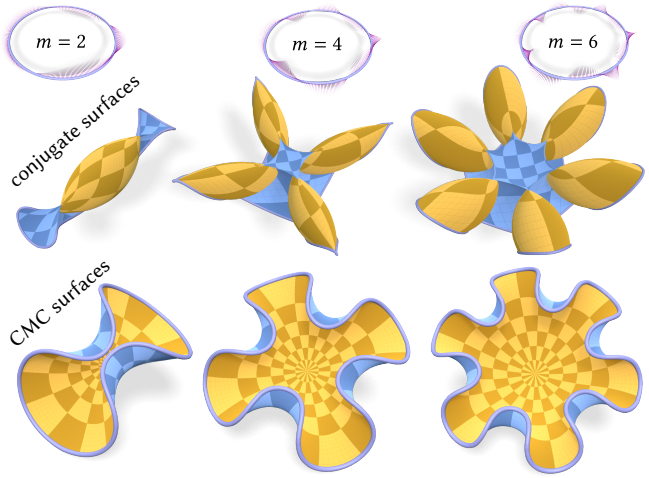

Fig. 3. **Symmetric Disks.** A family of rotationally symmetric CMC disks (*bottom row*) and constant Gauß curvature surfaces (*middle row*) can be obtained by the harmonic extension of the boundary normal vectors $N_0^{(m)}$ obtained by rotating the outward pointing normal vectors of the unit disk by the angle $m\,\theta$ around the boundary circle tangent vector (*top row*); the boundary circle is parameterized by the angle $\theta \in [0, 2\pi) \mapsto e^{i\theta} \in \mathbb{S}^1$.

2 Smooth CMC Surfaces

We will develop our proposed algorithm starting with the smooth theory before describing its discrete instantiation. For this we use $\mathbb{R}^3$-valued differential forms for which the multiplication underlying the wedge product is either the cross or inner product. To wit, let $\alpha, \beta \in \Omega^1(M;\mathbb{R}^3)$ then $(\alpha \wedge \beta)(X,Y) \coloneqq \alpha(X) \times \beta(Y) - \alpha(Y) \times \beta(X)$ while $\langle \alpha \wedge \beta \rangle(X,Y) \coloneqq \langle \alpha(X), \beta(Y) \rangle - \langle \alpha(Y), \beta(X) \rangle$. Now, let M denote a two-dimensional orientable manifold endowed with a fixed Riemannian metric and $f\colon M \to \mathbb{R}^3$ an immersed surface with *Gauß map* $N\colon M \to \mathbb{S}^2$ mapping a point to its normal vector. The starting point for our development is the connection between CMC surfaces and the harmonicity of their Gauß map:

Theorem 2.1 ([Ruh and Vilms 1970]). *An immersion $f\colon M \to \mathbb{R}^3$ has constant mean curvature if and only if its Gauß map is harmonic.*

Harmonicity. Harmonic maps between surfaces are critical points of their Dirichlet energy $\mathcal{E}(N) = \frac{1}{2}\|dN\|^2$, *i.e.*,

$$\mathring{\mathcal{E}}(N) = -\int_M \langle \mathring{N}, d * dN \rangle = 0. \tag{1}$$

Due to $|N| = 1$, admissible variations $\mathring{N}$ are orthogonal to N. Hence for criticality $d * dN$ must be parallel to N. Equivalently, using the Leibniz rule, N is harmonic when

$$0 = -N \times (d * dN) = -d(N \times *dN) \eqqcolon -d\tau, \tag{2}$$

where $\tau = N \times *dN \in \Omega^1(M;\mathbb{R}^3)$

Proposition 2.2. *If a smooth map $N\colon M \to \mathbb{S}^2$ is harmonic, locally there is a smooth map $g\colon M \to \mathbb{R}^3$ satisfying $dg = N \times *dN$. It is the unique solution (up to constants) of the Poisson equation $d *^{-1} dg = dN \wedge dN$ (with suitable boundary conditions).*

Proof. Being closed ($d\tau = 0$), τ has a (local) integral $g\colon M \to \mathbb{R}^3$, which solves (up to co-homology and suitable boundary conditions) the Poisson problem (see Appendix C)

$$d*^{-1}(dg = \tau) \implies d*^{-1}\,dg = d*^{-1}\,\tau = d(N \times dN) = dN \wedge dN. \quad \square$$

Remark 1 (Properties of g). *Wherever g is immersed, it has constant Gauß curvature $K \equiv 1$ and Gauß map N. Since $dN \wedge dN$ is parallel to N we also see that g itself is harmonic.*[1] *That it has Gauß curvature $K \equiv 1$ follows from the equality of the area forms induced by g and N*

$$dg \wedge dg = \tau \wedge \tau = (N \times *dN) \wedge (N \times *dN) = dN \wedge dN \tag{3}$$

where we used $*dN = -dN \circ J$ for J the complex structure compatible with the metric, satisfying $J \circ J = -Id$.

We call the $\mathbb{R}^3$-valued map g the (harmonic) conjugate of the $\mathbb{S}^2$-valued harmonic map N because the differential of g is obtained by rotating the differential of N with the aid of the Hodge star, as is done with the conjugation of $\mathbb{R}^2$-valued harmonic maps [Conway 1994] and minimal surfaces [Pinkall and Polthier 1993]. We point the interested reader to Hélein [2001] for additional perspectives on the harmonic conjugation of $\mathbb{S}^2$-valued maps.

Finally, to construct a CMC surface from the harmonic map we offset g in the normal direction. Define $f_\pm\colon M \to \mathbb{R}^3$ via

$$f_\pm \coloneqq g \pm N. \tag{4}$$

Proposition 2.3. *The offset surfaces $f_\pm\colon M \to \mathbb{R}^3$ are conformal immersions with Gauß map $\pm N$ and constant mean curvature $H \equiv \frac{1}{2}$.*

Proof. Conformality of $df_+ = \tau + dN$ follows from $N \times df_+ = -*df_+$. Noting that $q_+ \coloneqq \frac{1}{2}(-\tau + dN)$ is anti-conformal ($N \times q_+ = *q_+$) we have the unique decomposition of the Weingarten map into conformal and anti-conformal parts

$$dN = \tfrac{1}{2}(\tau + dN) + \tfrac{1}{2}(-\tau + dN) = \tfrac{1}{2}df_+ + q_+ \tag{5}$$

which shows the mean curvature H to be a constant $\frac{1}{2}$. Since f_- has Gauß map $-N$ both its conformality and $H \equiv \frac{1}{2}$ follow from the argument for f_+ after mapping $N \mapsto -N$. $\square$

This conjugation process reduces the problem of designing CMC surfaces to the intrinsic problem of designing $\mathbb{S}^2$-valued harmonic maps followed by integration of τ. Boundary conditions of the CMC surface are replaced with boundary conditions on the Gauß map.

Remark 2 (Mean curvature normalization). *The fact that we only produce CMC-$\frac{1}{2}$ surfaces is a particular choice of normalization. Rescaling these offset surfaces by $s > 0$ produces CMC surfaces $\frac{1}{s}f_\pm$ with the same shape and Gauß map, but with $H \equiv \frac{s}{2}$.*

3 Discrete CMC Surfaces

In the discrete setting, we will take $\mathsf{M} = (\mathsf{V}, \mathsf{E}, \mathsf{F})$ to be a connected, manifold, cellular decomposition of M endowed with a piecewise Euclidean metric specified by edge lengths $\ell\colon \mathsf{E} \to \mathbb{R}_{>0}$. We also denote the vertices, edges, and faces of M by $\mathsf{V}(\mathsf{M})$, $\mathsf{E}(\mathsf{M})$, and $\mathsf{F}(\mathsf{M})$, respectively, when we need to clarify the relevant complex. The boundary vertices will be denoted $\mathsf{V}(\mathsf{M})_\partial$.

[1] g is a harmonic map *onto* its image; it is not a harmonic map into $\mathbb{R}^3$

For a discrete version of the smooth theory (Section 2) we assume a triangle mesh, $\mathsf{M} = \mathsf{T}$, a Gauß map placing normals at vertices, $\mathsf{N}\colon \mathsf{V}(\mathsf{T}) \to \mathbb{S}^2$ and define the discrete Dirichlet energy as

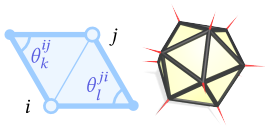

$$\mathcal{E}(\mathsf{N}) = \tfrac{1}{2}\sum_{ij} w_{ij}|\mathsf{N}_j - \mathsf{N}_i|^2 = \tfrac{1}{2}\langle\!\langle \mathsf{L}\mathsf{N}, \mathsf{N}\rangle\!\rangle \tag{6}$$

with $w_{ij} = \frac{1}{2}(\cot\theta_k^{ij} + \cot\theta_l^{ji})$ the usual cotangent weights, and L the cotangent Laplacian [MacNeal 1949; Pinkall and Polthier 1993]. A discrete map N is harmonic if it is a critical point of the discrete Dirichlet energy $\mathring{\mathcal{E}}(\mathsf{N}) = 0$ under all admissible variations, $\mathring{\mathsf{N}} \perp \mathsf{N}$.

Proposition 3.1. *A map $\mathsf{N}\colon \mathsf{V}(\mathsf{T}) \to \mathbb{S}^2$ is a discrete harmonic map if and only if for all interior vertices $i \in \mathsf{V}(\mathsf{T})$, $-\mathsf{N}_i \times (\mathsf{L}\mathsf{N})_i = 0$.*

Proof.

$$\begin{aligned}\mathring{\mathcal{E}}(\mathsf{N}) &= -\sum_{ij} w_{ij}(\langle \mathsf{N}_i, \mathring{\mathsf{N}}_j\rangle + \langle \mathring{\mathsf{N}}_i, \mathsf{N}_j\rangle)\\ &= \sum_i \langle \mathring{\mathsf{N}}_i, -\sum_{ij} w_{ij}\mathsf{N}_j\rangle = 0.\end{aligned} \tag{7}$$

Hence $\mathring{\mathcal{E}}(N) = 0$ when $\mathsf{N}_i \parallel \sum_{ij} w_{ij}\mathsf{N}_j$, which occurs when

$$\forall i \in \mathsf{V}(\mathsf{T})\colon\ -\mathsf{N}_i \times \sum_{ij} w_{ij}\mathsf{N}_j = -\mathsf{N}_i \times \sum_{ij} w_{ij}(\mathsf{N}_j - \mathsf{N}_i) = 0. \quad \square$$

Remark 3 (Fixed Edge Weights). *To compute the area of a discrete surface, one can compute the Dirichlet energy of the immersion using the cotangent weights induced by the surface itself—these cotangent weights change as the immersion changes. In contrast, our Dirichlet energy minimization problem is simpler in the sense that the cotangent weights used to define the Dirichlet energy do not depend on the variables we are optimizing.*

Equivalently, (trapezoid) integrating N along edge ij and moving it through the summation we find N to be a discrete harmonic map when

$$\forall i \in \mathsf{V}(\mathsf{T})\colon\ -\sum_{ij} \tfrac{\mathsf{N}_i + \mathsf{N}_j}{2} \times w_{ij}(\mathsf{N}_j - \mathsf{N}_i) = 0 \tag{8}$$

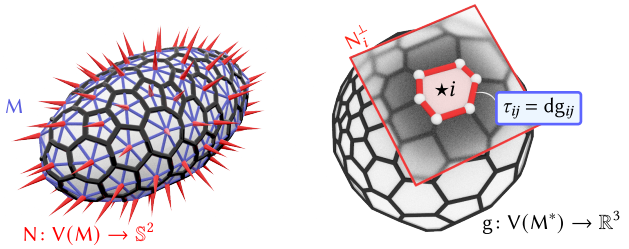

Fig. 4. **Discrete Conjugation.** The balancing condition that defines an $\mathbb{S}^2$-valued harmonic map can be interpreted geometrically as the closing up of a dual polygon for every vertex of M. In these cases, the edge vectors define a discrete conjugate surface of the harmonic map.

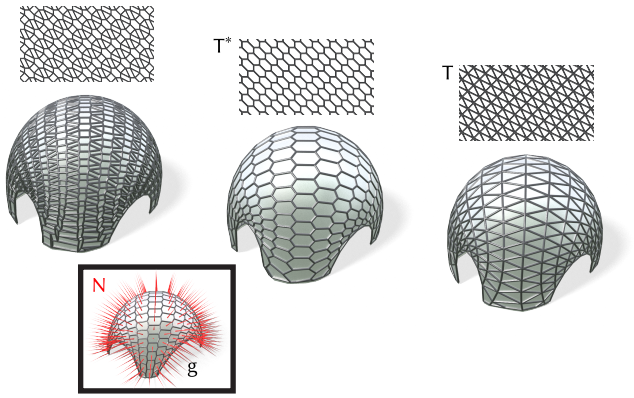

Fig. 5. **Combinatorics of the Offset.** Starting from the same discrete harmonic map N on a triangle mesh T, a discrete CMC surface is obtained as a vertex offset of the conjugate surface (*middle*) or its dual (*right*) by averaging N or g, respectively. Another natural complex to define a face offset is obtained by inserting new faces for each vertex and edge of T, with vertex set equal to the corners of T (*left*).

which is a Discrete Exterior Calculus (DEC) [Desbrun et al. 2008] version of $-d(N \times *dN) = -d\tau = 0$ for the discrete dual 1-form

$$\tau_{ij} \coloneqq \tfrac{\mathsf{N}_i+\mathsf{N}_j}{2} \times w_{ij}(\mathsf{N}_j - \mathsf{N}_i) = w_{ij}\mathsf{N}_i \times \mathsf{N}_j. \tag{9}$$

The dual Poisson equation for g also amounts to a DEC realization of $d *^{-1} dg = dN \wedge dN$:

Proposition 3.2. *If a discrete map* $\mathsf{N}\colon \mathsf{V}(\mathsf{T}) \to \mathbb{S}^2$ *is harmonic, locally there is a discrete map* $\mathsf{g} \in \Omega^0(\mathsf{T}^*;\mathbb{R}^3)$ *satisfying* $\mathrm{d}\mathsf{g} = \tau$. *It is the unique solution (up to constants) of the discrete (dual) Poisson equation* $\mathrm{d}^\top *^{-1} \mathrm{d}\mathsf{g} = \mathrm{d}\mathsf{N} \wedge \mathrm{d}\mathsf{N}$, *with* $(\mathrm{d}\mathsf{N} \wedge \mathrm{d}\mathsf{N})_{ijk} \coloneqq \sum_{ij} \mathsf{N}_i \times \mathsf{N}_j$.

Proof. The closure of τ (for all $i \in \mathsf{V}(\mathsf{T})$, $\sum_{ij} \tau_{ij} = 0$) certifies both the harmonicity of N and the (local) existence of an integral g. The τ_{ij} being dual edge vectors their integral g is located at dual vertices and solves (ignoring co-homology and boundary conditions for simplicity) a dual Poisson problem

$$\begin{aligned}\forall ijk \in \mathsf{V}(\mathsf{T}^*)\colon \sum_{*ij} w^*_{ij}(\mathsf{g}_{ijk} - \mathsf{g}_{jil}) &= \sum_{ij} \tfrac{\mathsf{N}_i+\mathsf{N}_j}{2} \times (\mathsf{N}_j - \mathsf{N}_i) \\ &= \sum_{ij} \mathsf{N}_i \times \mathsf{N}_j = 2\mathsf{K}_{ijk}\mathsf{N}_{ijk}\end{aligned} \tag{10}$$

where $w^*_{ij} \coloneqq w_{ij}^{-1}$ are the dual cotangent weights, K_{ijk} denotes the Euclidean area of the triangle formed by N_i, N_j, N_k, and N_{ijk} its normal. □

Geometrically the τ_{ij} form a closed polygon dual to vertex i (Figure 4). These polygons are planar since the edges are orthogonal to N_i, and they are realized by the dual vertex positions g.

Discrete CMC Offsets. We now have g and N after solving a nonlinear Laplace problem and a standard Poisson problem (see Section 4.2). Unfortunately, we cannot immediately form the CMC offset surfaces $f_\pm$ since g is defined on dual vertices, *i.e.*, triangles, while N is defined on primal vertices. We address this by averaging either g or N onto M or M^* so that we can define the offset surfaces with the combinatorics of either

$$\mathsf{A}\colon \Omega^0(\mathsf{T}^*) \to \Omega^0(\mathsf{T}), \quad \mathsf{A}(\mathsf{g})_i = \tfrac{1}{\sum_{ijk} A_{ijk}} \sum_{ijk} \mathsf{g}_{ijk} A_{ijk} \tag{11}$$

$$\mathsf{A}_*\colon \Omega^0(\mathsf{T}) \to \Omega^0(\mathsf{T}^*), \quad \mathsf{A}_*(\mathsf{N})_{ijk} = \tfrac{1}{\sum_{v\in\{i,j,k\}} A_v} \sum_{v\in\{i,j,k\}} \mathsf{N}_v A_v, \tag{12}$$

where A_v is the barycentric or Voronoi dual area of vertex $v \in \mathsf{V}(\mathsf{M})$. This enables us to define the offset surfaces (when $\mathsf{M} = \mathsf{T}$) as

$$\mathsf{f}_\pm = \mathsf{A}(\mathsf{g}) \pm \mathsf{N} \in \Omega^0(\mathsf{T};\mathbb{R}^3) \quad \text{or}$$
$$\mathsf{f}_\pm = \mathsf{g} \pm \mathsf{A}_*(\mathsf{N}) \in \Omega^0(\mathsf{T}^*;\mathbb{R}^3)$$

on the primal respectively dual mesh (see Figure 5).

Remark 4 (Non-trivial topology). *The discrete conjugate* g *arises in the Hodge decomposition* $\tau = \mathrm{d}\mathsf{g} + \eta$ *where* $\mathsf{g} \in \Omega^0(\mathsf{M}^*;\mathbb{R}^3)$ *and* $\eta \in \Omega^1(\mathsf{M}^*;\mathbb{R}^3)$ *is harmonic. When* M *is simply connected, there are no harmonic forms, and we obtain a bona fide discrete surface satisfying* $\mathrm{d}\mathsf{g} = \tau$. *Otherwise, the surface has translational periods, and a surface with differential equal to* τ *is only well-defined on the universal cover. Alternatively, the periodic conjugate surface can be computed using the Hodge decomposition after cutting* M *along homology generators (Section 5.3).*

4 Discrete CMC Surfaces with Generalized Combinatorics

Our construction of a discrete constant mean curvature surface only depends on a discrete harmonic map $\mathsf{N}\colon \mathsf{V}(\mathsf{M}) \to \mathbb{S}^2$, defined on a cell-complex. The most straightforward case, which we treated explicitly in Section 3, works with a triangle mesh, $\mathsf{M} = \mathsf{T}$, placing N at primal vertices. In some settings though it may be more natural to place normals N at faces $\mathsf{F}(\mathsf{T})$, *i.e.*, the vertices of $\mathsf{M} = \mathsf{T}^*$. The conjugate surface is then a triangle mesh (Figure 6). In this section, we describe the necessary changes to the construction when working with normals defined at the vertices of more general cell-complexes.

For a uniform treatment we replace the PL discretization of the Dirichlet energy with a function of the bending angles, *i.e.*, the change in normal, for every edge:

$$\mathcal{E}(\mathsf{N}) \coloneqq \sum_{ij\in\mathsf{E}} \epsilon_{ij}(\alpha_{ij}), \tag{13}$$

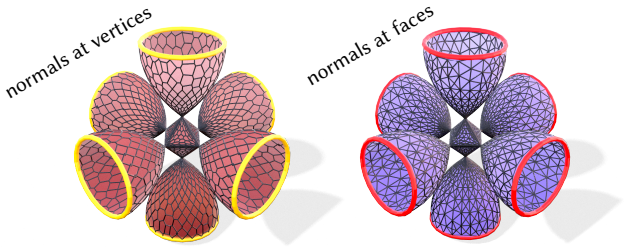

Fig. 6. **Combinatorics of Discrete K-Surfaces.** By starting with a discrete harmonic map defined on a triangle mesh or its dual, we obtain discretizations of surfaces with constant Gauß curvature that have the combinatorics of the dual or primal mesh, respectively.

where $\epsilon_{ij} \in C^2(\mathbb{R};\mathbb{R})$, and the bending angle $\alpha_{ij} \in [0,\pi]$ is defined by $\cos\alpha_{ij} = \langle \mathsf{N}_i, \mathsf{N}_j\rangle$. Concrete choices for ϵ_{ij} that discretize the Dirichlet energy are presented below.

As in the case when M is a triangulated surface, we can transform the associated discrete harmonic map equation (Proposition 4.1) into the integrability condition of an immersion—this is again a discrete version of the smooth theory from Section 2 where in both cases the integrability of g is simultaneously the condition for the Gauß map to be harmonic.

Proposition 4.1. *A discrete sphere valued map $\mathsf{N}\colon \mathsf{V} \to \mathbb{S}^2$ is a critical point of $\mathcal{E}$ if and only if for every vertex $i \in \mathsf{V}$,*

$$-\sum_{ij} \frac{\mathsf{N}_i+\mathsf{N}_j}{2} \times \frac{\epsilon'_{ij}(\alpha_{ij})}{\sin\alpha_{ij}}(\mathsf{N}_j - \mathsf{N}_i) = 0 \tag{14}$$

(cf., Equation 8). If the boundary values are held fixed, then this equation only needs to hold for each interior vertex.

To make the analogy with the smooth theory more immediate in the general setting, we consider a possibly non-linear Hodge star

$$(*_{\mathcal{E}})_{ij} \coloneqq \frac{\epsilon'_{ij}(\alpha_{ij})}{\sin\alpha_{ij}}.$$

Then Equation 14 is written

$$-\mathrm{d}(\mathsf{N} \times *_{\mathcal{E}} \mathrm{d}\mathsf{N}) = 0.$$

Since the closure of the dual one-form $\tau = \mathsf{N} \times *_{\mathcal{E}} \mathrm{d}\mathsf{N} \in \Omega^1(\mathsf{M}^*;\mathbb{R}^3)$ is equivalent to discrete harmonicity of N, we conclude:

Proposition 4.2. *If a discrete map $\mathsf{N}\colon \mathsf{V}(\mathsf{M}) \to \mathbb{S}^2$ is harmonic, then there exists locally a discrete map $\mathsf{g} \in \Omega^0(\mathsf{M}^*;\mathbb{R}^3)$ satisfying $\mathrm{dg} = \tau$.*

4.1 Discrete Harmonic Maps into $\mathbb{S}^2$

Each discretization of the Dirichlet energy gives rise to a different notion of discrete CMC surfaces via our construction. The primal cotangent Laplacian, for example, which produced the CMC surfaces described in Section 3, is given by

$$\epsilon^{\cot}_{ij}(\alpha_{ij}) = \tfrac{1}{2} w_{ij}(2\sin\tfrac{\alpha_{ij}}{2})^2 \qquad (\epsilon^{\cot}_{ij})'(\alpha_{ij}) = w_{ij}\sin\alpha_{ij},$$

and analogously for the dual cotangent Laplacian which replaces w_{ij} with $w^*_{ij} = \frac{1}{w_{ij}}$. Unfortunately the dual cotangent Laplacian is numerically brittle. On triangle meshes that are not intrinsically Delaunay the edge weights may be negative or infinite for configurations which have the four vertices of two triangles sharing an edge (nearly) co-circular. This motivates the search for a more numerically robust dual discrete Dirichlet energy.

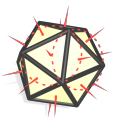

Discrete Willmore Energy. A more robust dual Dirichlet energy can be constructed based on the Möbius invariant discrete Willmore energy [Bobenko 2005; Bobenko and Schröder 2005]

$$\epsilon^{\mathrm{möb}}_{ij}(\alpha_{ij}) = 2(\beta_{ij}(\alpha_{ij}) + \theta^{ij}_k + \theta^{ji}_l - \pi) \tag{15}$$

where the angles θ^{ij}_k and θ^{ji}_l arise from the fixed metric of M and the circumcircle intersection angle β_{ij} is defined through

$$\cos\beta_{ij} = \sin\theta^{ij}_k \sin\theta^{ji}_l \cos\alpha_{ij} - \cos\theta^{ij}_k \cos\theta^{ji}_l.$$

Only β_{ij} is dependent on α_{ij} so that the derivative of $\epsilon^{\mathrm{möb}}_{ij}$ with respect to α_{ij} is given by

$$(\epsilon^{\mathrm{möb}}_{ij})'(\alpha_{ij}) = \frac{2\sin\theta^{ij}_k \sin\theta^{ji}_l}{\sin\beta_{ij}}\sin\alpha_{ij}. \tag{16}$$

Remarkably $\epsilon^{\mathrm{möb}}$ is always non-negative even for non-Delaunay triangle meshes making it our most numerically robust dual energy. We study this energy in more detail in Appendix A.

Remark 5 (Fixed Dual Edge Weights). *Analogous to the primal discretization of the Dirichlet energy, where the cotangent weights do not vary throughout optimization, the θ_{ij} variables used to define ϵ_{ij} above are also fixed. These corner angles are a function of the intrinsic metric of the input domain, which we do not vary. In the special case when the intrinsic metric is induced from vertex positions f and N is its discrete Gauß map, the Dirichlet energy $\mathcal{E}_{\mathrm{möb}}(\mathsf{N})$ computes the discrete Willmore energy (Proposition A.2).*

For completeness we mention two other common dual energies.

Discrete Bending Energies. One may also use the dihedral angle directly as is done for shells [Grinspun et al. 2003; Bridson et al. 2003]

$$\epsilon^{\mathrm{shell}}_{ij}(\alpha_{ij}) = \tfrac{1}{2} w^*_{ij}\alpha^2_{ij} \qquad (\epsilon^{\mathrm{shell}}_{ij})'(\alpha_{ij}) = w^*_{ij}\alpha_{ij}.$$

To avoid degeneracies as $\alpha_{ij} \to \pm\pi$ Bobenko and Suris [1999] suggest

$$\epsilon^{\tan}_{ij}(\alpha_{ij}) = 2\,w^*_{ij}\log(\sec\tfrac{\alpha_{ij}}{2})^2 \qquad (\epsilon^{\tan}_{ij})'(\alpha_{ij}) = 2\,w^*_{ij}\tan\tfrac{\alpha_{ij}}{2}.$$

Due to the superiority of $\epsilon^{\mathrm{möb}}$ among the dual Dirichlet energies (Section A.1) we do not pursue the other discrete bending energies further.

Remark 6. *A variety of edge weights have been proposed for measuring the Dirichlet energy over triangle meshes. For example, mean-value weights [Floater et al. 2006] or combinatorial weights (*i.e.*, all triangles are equilateral). In the context of unconstrained spherical parameterizations another discretization for $\mathbb{S}^2$-valued maps was proposed by Friedel et al. [2007] using locally rescaled edge weights to approximate the smooth Dirichlet energy from above. We leave the investigation of the resulting notions of discrete CMC surfaces to future work, and (when M is a triangle mesh) only consider the cotangent Laplacian in this work.*

4.2 Numerical Solution

With the discrete formulation at hand, we now proceed to its numerical solution. To compute harmonic maps we employ heat flow, *i.e.*, gradient descent of the Dirichlet energy [Eells and Sampson 1964]. Instead of the L^2-gradient though we use the Sobolev H^1-gradient with its enhanced convergence due to preconditioning [Eckstein et al. 2007; Neuberger 2010; Bartels 2015]. If desired, additional acceleration can be achieved using Newton's method near a critical point (Appendix B).

Harmonic Map Heat Flow. Let $\mathcal{M} \subset \Omega^0(\mathsf{M};\mathbb{S}^2)$ denote the manifold of all discrete $\mathbb{S}^2$-valued maps N satisfying specified Dirichlet boundary conditions on a subset of the boundary $\Gamma_D \subset \mathsf{V}(\mathsf{M})_\partial$.

The tangent space at a point $\mathsf{N} \in \mathcal{M}$ is given by variations $\mathring{\mathsf{N}}_i \perp \mathsf{N}_i$ and vanishing on Γ_D. To integrate a tangent vector while staying on $\mathbb{S}^2$ we use the exponential map—it is given by applying the exponential map on $\mathbb{S}^2$ at each vertex:

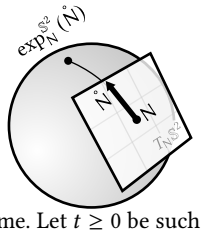

$$\exp^{\mathcal{M}}_{\mathsf{N}}(\mathring{\mathsf{N}})_i \coloneqq \exp^{\mathbb{S}^2}_{\mathsf{N}_i}(\mathring{\mathsf{N}}_i).$$

We may now take discrete steps in (pseudo-)time. Let $t \geq 0$ be such a discrete time index, and consider a point $\mathsf{N}^t \in \mathcal{M}$. The update direction $\delta\mathsf{N}^t \in T_{\mathsf{N}^t}\mathcal{M}$ is found by solving

$$\forall \varphi \in T_{\mathsf{N}^t}\mathcal{M}: \quad \langle\!\langle \delta\mathsf{N}^t, \varphi \rangle\!\rangle_{H^1} + \langle\!\langle \operatorname{grad} \mathcal{E}(\mathsf{N}^t), \varphi \rangle\!\rangle = 0, \tag{17}$$

where $\operatorname{grad} \mathcal{E}(\mathsf{N}^t)_i = (\mathsf{L}\mathsf{N}^t)_i$ and $\langle\!\langle \psi, \varphi \rangle\!\rangle_{H^1} \coloneqq \langle\!\langle (*_0 + \mathrm{d}^\top *_1 \mathrm{d})\psi, \varphi \rangle\!\rangle$ is the discrete H^1-inner product using DEC and the usual cotangent Hodge-$*$. Taking an explicit time step $h > 0$ we obtain a new point $\mathsf{N}^{t+h} \in \mathcal{M}$:

$$\mathsf{N}^{t+h} = \exp^{\mathcal{M}}_{\mathsf{N}^t}(h\,\delta\mathsf{N}^t),$$

where backtracking line search on h ensures that the energy decreases at each iteration.

Remark 7. *Although the piecewise linear interpolant does not satisfy the unit norm constraint inside the triangles, minimizing this piecewise linear discretization of the Dirichlet energy with the values at vertices constrained to $\mathbb{S}^2$ is known to approximate $\mathbb{S}^2$-valued harmonic maps [Bartels 2015, Theorem 7.6].*

Remark 8. *A variety of alternatives can be used to minimize the Dirichlet energy, including minimization of a Ginzburg-Landau type relaxation [Monteil et al. 2021]. To avoid sparse linear algebra altogether, one can also apply a nonlinear Gauss-Seidel approach, iteratively averaging at a vertex i the neighboring normals (Equation 7):*

$$\mathsf{N}_i \leftarrow \frac{n}{|n|} \quad n \leftarrow -\sum_{ij} w_{ij} \mathsf{N}_j.$$

While it converges strictly slower than the H^1-gradient flow, this scheme is both simple to implement and robust.

With a discrete harmonic N in hand we can assemble the right hand side of the Poisson problem for g (Equation 10) and solve it.

4.3 Practicalities

4.3.1 Boundary Considerations. The edge vectors τ_{ij} surrounding a boundary vertex i do not usually form a closed polygon. To obtain a regular boundary curve, we augment τ to close the faces around the boundary vertices as well. For $\mathsf{M} = \mathsf{T}$ we close the dual polygons for boundary vertices $\mathsf{V}(\mathsf{T})_\partial$ by adding new vertices and faces (Figure 7, top). For $\mathsf{M} = \mathsf{T}^*$, boundary vertices in M correspond to faces $\mathsf{F}(\mathsf{T})$ incident to a boundary edge, and we define τ on this edge (Figure 7, bottom).

4.3.2 The Shape Operator. To evaluate our algorithm we need a numerical approximation of the shape operator $S\colon TM \to TM$ of an immersion f. Recall that S is a symmetric linear map defined by $dN = df \circ S$ and encodes the curvature. To evaluate the mean curvature and principal curvature directions of our discrete triangle meshes ($\mathsf{M} = \mathsf{T}$), we

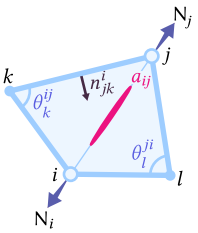

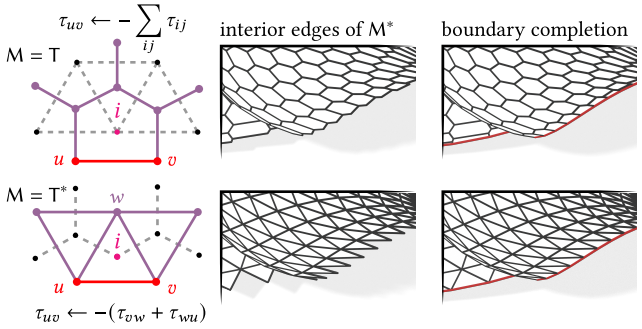

Fig. 7. **Boundary Conjugation.** To complete the dual face associated to a boundary vertex of M we define τ along a single additional edge (red) so that the edge vectors sum to zero.

follow Corman [2024, Sec. 4.1] and approximate the shape operator using the lowest order Regge finite elements

$$\mathcal{S}^k_{ij} \coloneqq -\frac{n^i_{jk} \otimes n^i_{ki} + n^j_{ki} \otimes n^j_{jk}}{2 \sin\theta^{jk}_i \sin\theta^{ki}_j},$$

where n^i_{jk} is the 90° rotated (in the tangent space of ijk) unit vector t_{jk} in the direction of the edge jk, and θ^{jk}_i is the corner angle opposite jk. These finite elements span the space of piecewise constant, in each face ijk, symmetric matrices

$$\mathsf{S}_{ijk} \coloneqq a_{ij}\mathcal{S}^k_{ij} + a_{jk}\mathcal{S}^i_{jk} + a_{ki}\mathcal{S}^j_{ki}$$

interpolating given edge data since $\mathcal{S}^k_{ij}(t_{ij}, t_{ij}) = 1$ and $\mathcal{S}^k_{ij}(t_{jk}, t_{jk}) = \mathcal{S}^k_{ij}(t_{ki}, t_{ki}) = 0$, and correspondingly for the other two edges in triangle ijk. The coefficients for the shape operator on each edge $ij \in \mathsf{E}$ are given by the discrete normal curvature along the edge

$$a_{ij} \coloneqq \tfrac{1}{|\mathrm{d}\mathsf{f}_{ij}|^2} \langle \mathrm{d}\mathsf{N}_{ij}, \mathrm{d}\mathsf{f}_{ij} \rangle.$$

Validating our discretization, we plot the distribution of the mean curvature and plot streamlines of the principal curvature directions, both approximated using S_{ijk}, in Figure 8.

4.3.3 Intrinsic Triangulations. The discretization of the Dirichlet energy only depends on the intrinsic geometry of the underlying triangle mesh, reflecting the corresponding dependence only on the metric in the smooth setting—the Dirichlet energy only depends on the conformal type. Therefore, it is possible to further improve accuracy and robustness by using the intrinsic Delaunay triangulation [Sharp et al. 2019; Gillespie et al. 2021].

5 Designing CMC Surfaces

With the forward construction of discrete constant mean curvature surfaces from a harmonic $\mathbb{S}^2$-valued map under our belt, we now turn our attention to the constrained variational problems needed to design CMC surfaces. Because our representation is based on the Gauß map rather than the immersion itself, the relevant variational problems differ from volume-constrained area minimization: the design variables are boundary normals, and the target space consists of harmonic maps into $\mathbb{S}^2$. We focus on the applications and the essential concepts and formulate these optimization problems in the smooth setting (see Section 4.2 for details in the discrete setting).

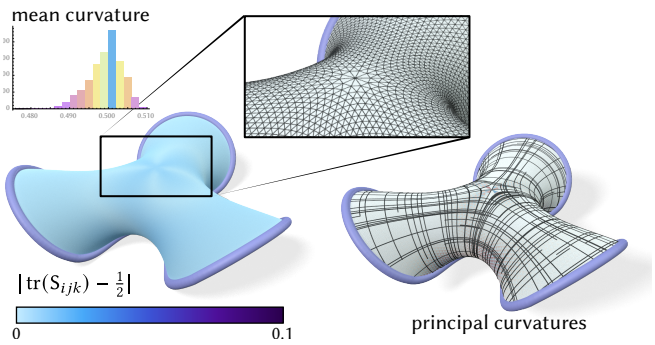

Fig. 8. **Numerical Validation.** Our discretization produces excellent approximations of smooth CMC surfaces. We use the Regge finite-elements to approximate the shape operator. It gives pointwise approximations of the mean curvature (*left*) and principal curvature directions (*right*) in each face. We plot the distribution of this discrete mean curvature (histogram bars colored by height), and find that it clusters around $^1/_2$ with standard deviation 0.004.

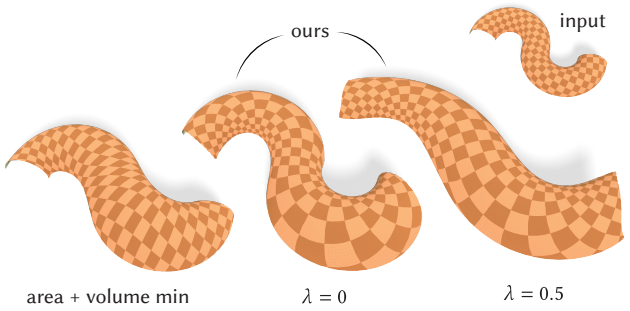

Fig. 10. **CMC Approximation of a Smooth Surface.** By identifying CMC disks with harmonic maps, our method enables exploration of the entire landscape of constant mean curvature surfaces which are topological disks. The CMC approximation obtained by fixing the boundary and minimizing the area constrained with the same volume as the input distorts the parameterization non-conformally (*left*). Our approximations are conformal and optimal in that we minimize the deviation from the Gauß map of the input (*middle*), additionally penalizing variations of the normal along the boundary (*right*).

Algorithm 1 BoundaryNormalsToCMC

Input: A simply connected mesh M with boundary normals N_0
Output: A pair of discrete CMC surfaces $f_\pm : V(M) \to \mathbb{R}^3$
1: Compute a harmonic extension $N : V(M) \to \mathbb{S}^2$ of N_0
2: Compute the conjugate g satisfying $dg = \tau$ on M^*
3: Construct the primal offset surfaces $f_\pm = A(g) \pm N$

5.1 Tangent Plane Boundary Conditions

The simplest way to design a sphere valued harmonic map is to minimize the Dirichlet energy subject to Dirichlet boundary conditions:

$$\min_{N:\, M\to\mathbb{S}^2} \mathcal{E}(N) := \tfrac{1}{2}\|dN\|^2 \quad \text{subject to} \quad N|_{\partial M} = N_0 : \partial M \to \mathbb{S}^2.$$

The Dirichlet boundary conditions on N fix the tangent planes along the boundary, as in Figure 1 and Figure 3. Natural choices for the boundary conditions, when an immersion is given, include the Gauß map itself or the binormals (Figure 2). Homogeneous Neumann boundary conditions, $\partial N/\partial \nu = 0$ with ν the inward pointing normal of ∂M, can also be incorporated on a subset of the boundary by simply allowing N to be free variables there in the optimization problem above.

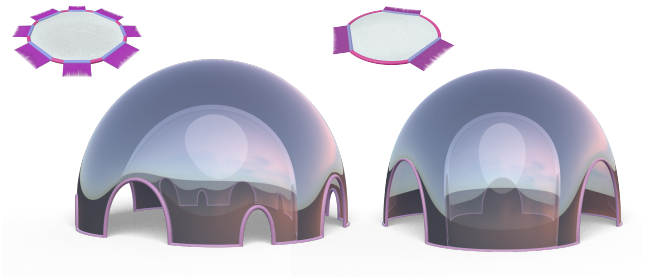

Fig. 9. **CMC Surfaces with Planar Boundaries.** Prescribing a constant Gauß map on a boundary component makes the surface tangential to a plane there (the vertical boundary components); prescribing a reflectional symmetry makes the surface orthogonal to a plane (the ground plane curves).

5.1.1 Surfaces Touching a Plane. CMC surfaces that touch a plane, either tangentially or orthogonally, can be easily designed using the normal representation. Specifying a constant Gauß map $N|_\Gamma = c$ along a boundary component Γ forces the resulting surface to be tangential to a plane orthogonal to c along Γ. To specify that the surface cuts a plane orthogonally we instead impose a symmetry constraint. By the Schwarz reflection principle, if some part of the boundary of a CMC surface lies in a plane and the surface is orthogonal to that plane, the CMC surface can be extended by reflection in the plane. We can specify such a reflectional symmetry (fixing the reflecting plane up to a translation) by computing, during minimization, the Dirichlet energy of N as if the surface were in fact continued through the corresponding reflectional symmetry on $\mathbb{S}^2$. Both of these boundary conditions are illustrated in the example in Figure 9. These CMC surfaces are simpler to fabricate since the boundary support structures lie in a plane.

5.2 Surface Approximation

We can approximate an arbitrary smooth immersion $\varphi : M \to \mathbb{R}^3$ of a disk M by a CMC surface by solving the following optimization problem. It is defined by an energy functional $\mathcal{F}$ for the Dirichlet boundary conditions and its harmonic extension to the interior

$$\min_{N_0:\, \partial M\to\mathbb{S}^2} \mathcal{F}(N_0, N)$$
$$\text{subject to} \quad N|_{\partial M} = N_0 \text{ and } N \text{ is harmonic.}$$

We consider the explicit energies

$$\mathcal{F}_\lambda(N_0, N) = \|N - N_\varphi\|^2_{L^2} + \lambda\|dN_0\|^2_{L^2(\partial M)}$$

so that we best approximate the Gauß map of our input surface while penalizing variations in the normals along the boundary (Figure 11). Increasing λ prefers smoother tangent planes along the boundary and regularizes the inverse problem (Figure 10). We give an explicit expression for the gradient of the reduced functional (in the discrete setting) in Appendix F, which we use for minimization via gradient descent.

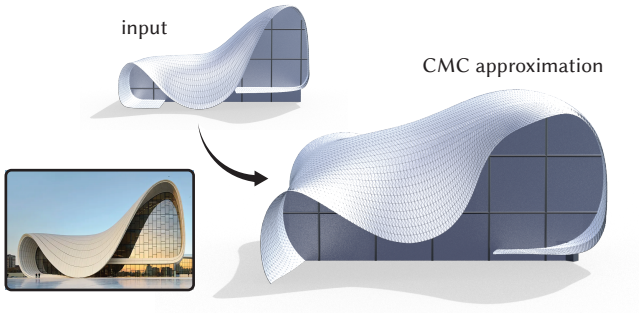

Fig. 11. **CMC from Architecture.** Starting from an input surface (*top left*), modeled on the Heydar Aliyev Center in Baku, Azerbaijan (*bottom left*), we approximate it as a CMC surface by projecting its Gauß map onto the space of $\mathbb{S}^2$-valued harmonic maps. The resulting surface achieves a small constant mean curvature, reproducing the nearly flat base of the surface. *Photograph courtesy of Hufton+Crow*

5.3 Periodic CMC Surfaces

We now turn to the design of periodic constant mean curvature surfaces. While area and volume based methods are limited to solving the Plateau problem for CMC surfaces with boundary, our construction allows us to explore the rich space of periodic and symmetric CMC surfaces by manipulating the topology, conformal structure of the domain, and symmetries on the Gauß map.

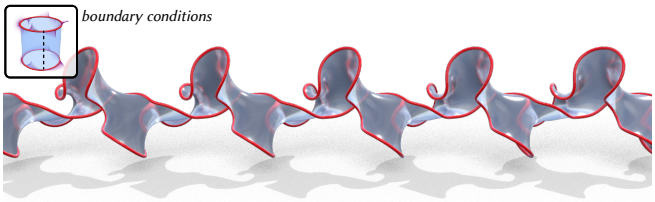

Fig. 12. **Infinitely Periodic Cylinders.** Periodic CMC surfaces can be obtained using harmonic maps into $\mathbb{S}^2$ defined on non-simply connected domains. Here, we consider the harmonic extension of normal vectors that wind around the cylinder's boundary to obtain this periodic CMC sheet.

5.3.1 Translational Periods and Cohomology. For a simply connected domain M, the condition $d\tau = 0$ is sufficient to guarantee the existence of the conjugate surface g. However, for non-simply connected domains, the integrability of g (and thus the CMC surfaces $f_\pm$) is obstructed by the cohomology of the 1-form τ. If we cut the domain into a topological disk along a basis of non-contractible loops $\{\gamma_i\}_{i=1}^{2g+b-1}$, the conjugate surface g will be well-defined on the fundamental domain and will exhibit a translational jump across the cuts. The *period vector* associated with a loop γ_i is given by

$$\mathbf{p}_i(N) \coloneqq \int_M \tau(N) \wedge \eta_i,$$

where η_i is the harmonic 1-form dual to γ_i[2]. The simplest example occurs when M is cylindrical since there is only a single period vector—in the periodic examples in Figures 12 and 13 we specify boundary conditions for the Gauß map, and obtain a constant mean curvature strip after cutting and tiling the fundamental domain. For the generated surface to be closed (*e.g.*, a cylinder or torus) we will need to enforce the periodicity condition $\mathbf{p}_i(N) = 0$.

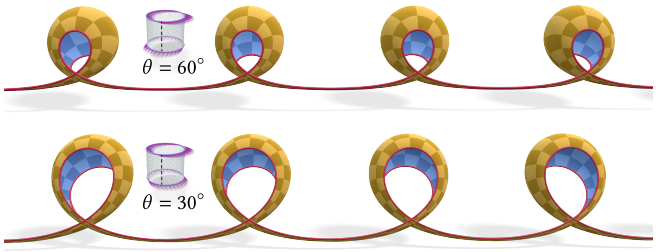

Fig. 13. **Discrete Wente Family.** Singly periodic CMC surfaces with boundary, like these discrete approximations of the Wente family, are obtained by computing harmonic maps on cylinders. After cutting the cylinder into a flat sheet, the domain and the harmonic map can be extended into data on an infinite sheet. These surfaces are obtained by taking constant normals on each boundary component that are separated by an angle θ (see inset).

5.3.2 Extension by Reflection. Many intricate periodic surfaces can be obtained by computing a fundamental piece between planes and extending it via reflection or rotation—see Appendix G. For instance, the Delaunay nodoids (Figure 14) are generated by solving for a harmonic map on a cylinder with boundary conditions

$$N|_{\Gamma_1} = e_1, \qquad N|_{\Gamma_2} = -e_1.$$

To generate the complete surface, we glue together the offsets $f_\pm$ periodically *à la* Theorem G.1. By varying the aspect ratio of the cylinder, we recover the complete one-parameter family of nodoids.

5.3.3 Optimizing the Conformal Type. The period vectors $\mathbf{p}_i$ depend not only on the boundary conditions, but also on the underlying conformal structure of the domain. This dependency provides the degree of freedom required to close the periods and construct closed constant mean curvature surfaces on multiply connected domains.

We focus on the case of a topological cylinder, which is conformally equivalent to a rectangular domain $[0, 2\pi] \times [0, h]$ with the vertical edges identified. The aspect ratio h is known as the conformal modulus of the cylinder. For a fixed set of boundary conditions $N_0 \colon \partial M \to \mathbb{S}^2$ we let N_h denote the harmonic extension computed on the domain with conformal modulus h, and since the domain is cylindrical there is a single period vector obtained by integrating τ

[2]when τ is closed, $\mathbf{p}_i(N)$ can also be computed by integrating τ over a closed curve. This, however, can be numerically delicate.

along the curve $\gamma = S^1 \times \{0\}$. To close the period $\mathbf{p}$, we look for a zero of the map

$$h \mapsto \mathbf{p}(N_h)$$

using Newton's method. Similar to the inverse design problem (Section 5), the derivative of the mapping in the discrete setting can be computed via the implicit function theorem as described in Appendix F. For the discrete Wente torus shown in Figure 15, we are required to close the gap in the periodic array of bubbles visualized in Figure 13–Newton's method reduces the norm of the period vector to machine precision in fewer than five iterations.

The principle extends to higher genus surfaces (Figure 16) by parameterizing the domain using multiple moduli (*e.g.*, lengths of cylindrical tubes in a polyhedral decomposition; inset, dashed lines).

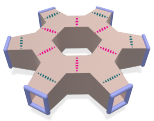

5.3.4 Balanced Gauß Maps. To robustly compute non-trivial harmonic maps from closed surfaces, such as those in Figures 13 and 15, we impose an additional constraint. Simply minimizing the Dirichlet

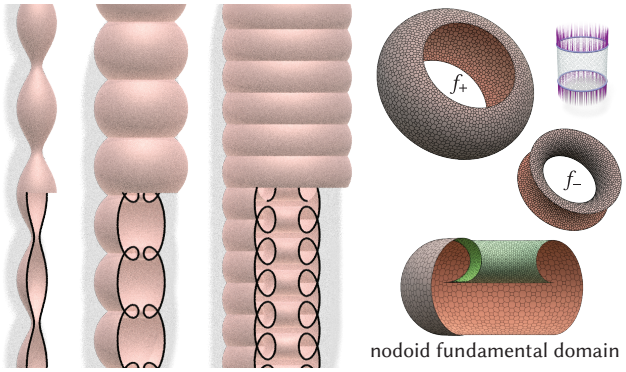

Fig. 14. **Unduloids and Nodoids.** The Gauß map of the nodoids (*right two*) arises by harmonic extension of opposing boundary normals (purple). The fundamental domain is obtained by gluing the f_+ and f_- surfaces along their boundaries. A one-parameter family of them is obtained by simply changing the conformal structure. The Gauß map of an unduloid (*left*) arises as the harmonic map connecting two latitude circles in $\mathbb{S}^2$.

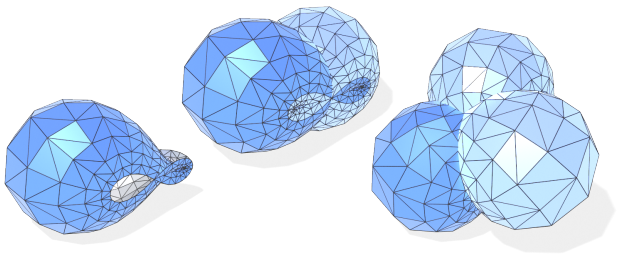

Fig. 15. **Discrete Wente Torus.** The Gauß map of the Wente torus can be approximated by minimizing the Dirichlet energy over maps from a cylinder with appropriate symmetries. The fundamental domain is illustrated in dark blue on the left. It has constant boundary normals 60° apart. Our discrete Wente torus is then obtained by rotating additional copies of the fundamental domain by 120°.

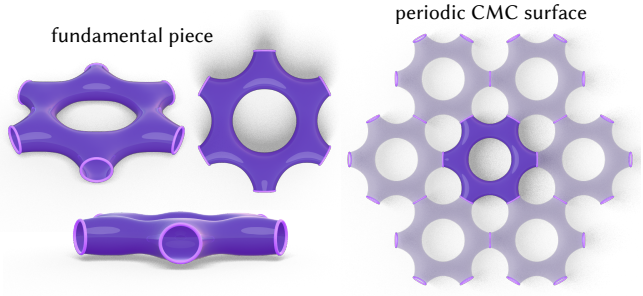

Fig. 16. **Periodic Closed Surfaces.** A closed periodic CMC surface constructed from a genus-one domain with six boundary components. Symmetry constraints on the Gauß map ensure the surface admits a reflectional symmetry about a horizontal plane, a rotational symmetry about a vertical axis, and orthogonally cut a plane along each boundary component. Closing the periods by optimizing over the conformal type produces a surface that tiles space by translation, forming a honeycomb-like lattice structure.

energy globally yields the trivial solutions $N \equiv$ constant[3], which produces a trivial map $f_\pm \equiv$ constant. To prevent concentration to a constant map, we add the constraint that the center of mass of N vanishes:

$$\int_M N \, \mu = 0,$$

where $\mu = \langle dN \wedge *dN \rangle \in \Omega^2(M; \mathbb{R})$ is the Dirichlet energy density of the map. We call such maps *balanced*. The Gauß map of a closed surface is always balanced, and we prove that it is also balanced for the periodic CMC surfaces produced by our construction[4] (Theorem E.1).

6 Evaluation

We evaluate the performance and accuracy of our discretization and algorithm on a diverse set of numerical experiments, focusing on computational efficiency, geometric fidelity, and mesh quality.

Approximation Quality. We validate the discrete properties of our generated surfaces across three discretizations of the Dirichlet energy presented in Section 4.1: $\mathcal{E}_{\text{cot}}$ on the primal and dual meshes, and $\mathcal{E}_{\text{möb}}$. First, we verify the constant mean curvature property by measuring the deviation of the discrete mean curvature as the trace of the shape operator (Section 4.3.2) from the target value $H = \frac{1}{2}$. As shown in Figure 17, the L^2 and L^∞ error converge linearly under mesh refinement. Next, we evaluate the conformal distortion from the input domain induced by the parameterizations $f_\pm$. We measure the L^2 error of the quasi-conformal distortion $\mathcal{Q}$ (*i.e.*, the ratio between the largest and smallest singular value of the deformation) and find that $\mathcal{Q} \approx 1$ is well-satisfied even on coarse meshes, and converges quadratically under refinement. While all discretizations are convergent we consistently observed that, over the dual mesh, the approximation error in the mean curvature is typically $\approx 20\%$ lower when using $\mathcal{E}_{\text{möb}}$ rather than the dual $\mathcal{E}_{\text{cot}}$; this is in addition

[3] see also [Friedel et al. 2007] for a discussion of a similar concentration phenomenon in the context of spherical parameterization

[4] compare this with a plane, which can be interpreted as a CMC-0 surface with translational periods, whose Gauß map is constant and therefore not balanced

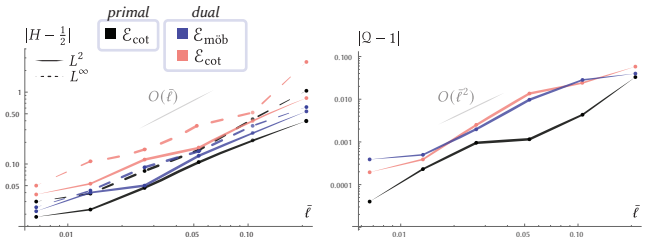

Fig. 17. **Convergence Under Refinement.** Here we plot the L^2 and L^∞ errors in the mean curvature (*left*) and the L^2 error of the quasi-conformal error (*right*) of the discrete CMC surfaces averaged over the three examples from Figure 3. Our discretization produces discrete CMC surfaces which converge to smooth CMC surfaces at a linear rate. In addition to the improved robustness afforded by using $\mathcal{E}_{\text{möb}}$ to measure the Dirichlet energy over the dual mesh, it also provides a more accurate approximation compared to discretizations based on the inverse of edge cotangent weights

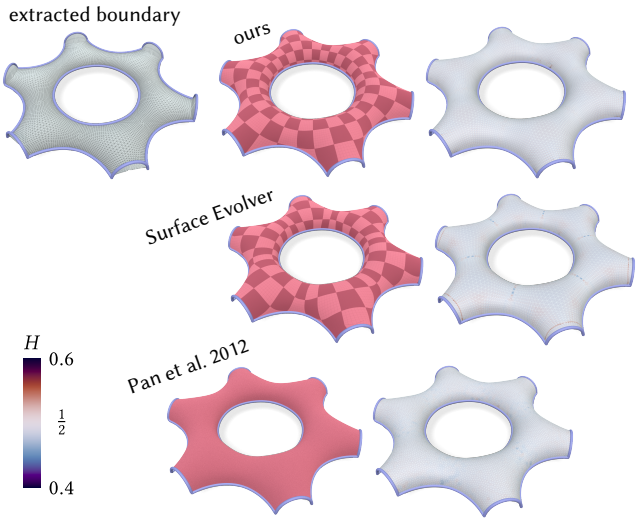

Fig. 18. **Comparison with Prior Work.** Our method (*top row*) produces approximations that are consistent with the algorithms of Brakke [1992] (*middle row*) and Pan et al. [2012] (*bottom row*). Unlike our method, which preserves the conformal structure of the input domain, the algorithm of Pan et al. [2012] does not keep track of any mapping to the input, while the algorithm of Brakke [1992] accumulates distortion in the parameterization due to tangential sliding.

to the improved robustness that is afforded by avoiding the inverse cotangent weights (see also Section A.1). Under mild assumptions on mesh quality, discrete harmonic maps into $\mathbb{S}^2$ are known to converge to smooth harmonic maps for the PL finite-element discretization under refinement. Since our discrete conjugate surfaces have Gauß maps equal to discrete harmonic maps by construction, we expect the conjugate surfaces—and hence the CMC offsets—to converge as well.

Consistency with Prior Work. Direct comparison with the algorithms of Pan et al. [2012] or Brakke [1992] is not possible due to the differing boundary value problems we solve (tangent planes vs. vertex positions). To bridge the gap, we perform a consistency check by (1) generating a CMC surface S using our method with fixed boundary normals starting from a planar reference domain, (2) extracting the boundary curve ∂S and the enclosed volume V, and (3) using these as input to the previous algorithms to generate a discrete surface $\tilde{S}$. We initialize their method with the planar domain modified at the boundary to agree with ∂S in Figure 18. We find that the surfaces are geometrically consistent, both exhibiting a Hausdorff distance $\approx 10^{-3}$ relative to the size of the bounding box diameter. Since the method of Pan et al. [2012] relies on dynamic remeshing to prevent degeneracy, it produces an isotropic mesh. However, these topological modifications destroy the correspondence with the input domain. Without remeshing, the method of Brakke [1992] accumulates additional tangential distortion since it makes no effort to preserve the conformal structure in the parameterization. In contrast, our method preserves the conformal structure that facilitates the transfer of UV parameterizations and other signals from the input domain.

Triangulation Quality Dependence. Our discretization of $\mathbb{S}^2$-valued harmonic maps inherits the same robustness of the cotangent based discretization of the Laplacian. In particular, our discretization of harmonic conjugation performs well even on irregular tesselations without any remeshing or preprocessing (Figure 19). While the input triangulation quality is unchanged in the final CMC surface, the underlying geometry is correctly captured nonetheless.

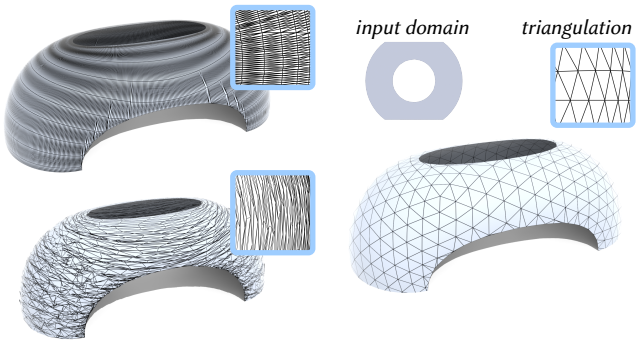

Fig. 19. **Mesh Quality Dependence.** Even when working with highly anisotropic and irregular triangulations (*left*) we reconstruct the same CMC surface computed with a highly regular triangulation (*right*). As we produce conformally parameterized surfaces, the imperfections of the input triangulation are preserved in the output.

Performance. The iterations of our optimization are dominated by the solution of a Poisson-like system (Section 4.2), which we solve using a Cholesky factorization. The Newton updates require the solution of a system of size $4|V|$ (for the vertex based discretization). We precompute the symbolic factorization of this matrix via PARDISO [Alappat et al. 2020], and update the numerical factorization in further iterations. On a typical model of about 50k vertices, we compute a minimizer of the Dirichlet energy with fixed Dirichlet boundary values within 1s; we terminate the optimization when the

L^2-norm of $\mathrm{N} \times (\mathrm{d} * \mathrm{dN})$ is below 10^{-6}. We implemented our solver in C++, and timings are reported on an Intel i7-14700K CPU.

7 Future Work

Our work suggests several questions and interesting directions for future work.

Boundary Control. A better understanding of the gap between tangent plane boundary conditions and the inputs typically specified in geometric modeling, such as boundary curves or enclosed volumes, would extend the applicability of our solver. Yet this change in perspective also opens new doors: *e.g.*, the construction of periodic CMC surfaces. While our surface approximation formulation generalizes in a straightforward manner for these other geometric targets, understanding the underlying relationship between boundary curves and boundary normals may further simplify these problems.

Discrete Mean Curvature. The discrete CMC surfaces we studied are defined through the conjugation and offset construction, but it remains open whether they admit a complementary notion of discrete mean curvature that is exactly constant. While our discretization of the conjugation process mimics the smooth setting, the offset construction involves an averaging operation whose geometric meaning deserves further study. More broadly, it would be valuable to understand how these discrete CMC surfaces relate to other notions in the literature—*e.g.*, those arising from area minimization or discrete integrable systems—toward a unified theory of polyhedral surfaces with distinguished curvature properties.

Minimal Surfaces and Willmore Surfaces. We studied discrete harmonic maps into the two-sphere and their relationship to CMC surfaces, but other distinguished surface classes can also be characterized by an associated harmonic map. For instance, Willmore surfaces have a harmonic sphere congruence (the mean curvature spheres). Inspired by this fact, we are interested in designing Willmore surfaces by first computing such harmonic maps and discretizing a conjugation and offset analogous to our CMC construction. Such an approach could provide a simple and robust alternative to Willmore flow—potentially opening the door to exploring symmetric and periodic Willmore surfaces, along with Willmore surface approximation by optimization over harmonic sphere congruences.

Minimal surfaces are also characterized by having a holomorphic Gauß map, along with a recently established structure-preserving discretization on arbitrary triangle meshes [Lam and Yasumoto 2025]. Generalizing our method, by incorporating discretizations of the Hopf differential, is a compelling way towards the computational exploration of symmetric and periodic minimal surfaces.

Acknowledgments

We thank Albert Chern for the early discussions during which the Möbius geometric discretization of the dual Dirichlet energy emerged. This work was supported in part by the Hausdorff Center for Mathematics at the University of Bonn, the Deutsche Forschungsgemeinschaft (DFG - German Research Foundation) - Project-ID 195170736 - TRR109 "Discretization in Geometry and Dynamics," and [EXC-2047/2 390685813]. Additional support was provided by SideFX software.

References

Christie Alappat, Achim Basermann, Alan R. Bishop, Holger Fehske, Georg Hager, Olaf Schenk, Jonas Thies, and Gerhard Wellein. 2020. A Recursive Algebraic Coloring Technique for Hardware-Efficient Symmetric Sparse Matrix-Vector Multiplication. *ACM Trans. Par. Comput.* 7, 3 (2020). doi:10.1145/3399732

Marc Alexa and Max Wardetzky. 2011. Discrete Laplacians on General Polygonal Meshes. In *Proc. ACM/SIGGRAPH Conf.* 1–10. doi:10.1145/1964921.1964997

Sören Bartels. 2015. *Numerical methods for nonlinear partial differential equations.* Vol. 47. Springer-Verlag.

Alexander Bobenko. 2005. A conformal energy for simplicial surfaces. *Comb. Comp. Geom.* 52 (2005), 133–143.

Alexander Bobenko and Ulrich Pinkall. 1996. Discrete surfaces with constant negative Gaussian curvature and the Hirota equation. *J. Diff. Geom.* 43, 3 (1996), 527–611.

Alexander Bobenko and Peter Schröder. 2005. Discrete Willmore flow. In *Proc. Symp. Geom. Proc.* 101–110.

Alexander Bobenko and Yuri Suris. 1999. Discrete Time Lagrangian Mechanics on Lie Groups, with an Application to the Lagrange Top. *Comm. Math. Phys.* 204 (1999), 147–188.

Alexander I Bobenko, Tim Hoffmann, and Nina Smeenk. 2024. Constant mean curvature surfaces from ring patterns: Geometry from combinatorics. *arXiv preprint arXiv:2410.08915* (2024).

Ossian Bonnet. 1853. Sur une propriété de maximum relative à la sphère. *Nouv. Ann. de Math* 12 (1853), 433–438.

Sofien Bouaziz, Mario Deuss, Yuliy Schwartzburg, Thibaut Weise, and Mark Pauly. 2012. Shape-up: Shaping discrete geometry with projections. *Comp. Graph. Forum* 31, 5 (2012), 1657–1667. doi:10.1111/j.1467-8659.2012.03171.x

Kenneth A Brakke. 1992. The Surface Evolver. *Experiment. Math.* 1, 2 (1992), 141–165. doi:10.1080/10586458.1992.10504253

Robert Bridson, Sebastian Marino, and Ron Fedkiw. 2003. Simulation of Clothing with Folds and Wrinkles. In *Proc. Symp. Comp. Anim.* 28–36. doi:10.2312/SCA03/028-036

Astrid Bunge, Philipp Herholz, Misha Kazhdan, and Mario Botsch. 2020. Polygon Laplacian Made Simple. 39, 2 (2020), 303–313. doi:10.1111/cgf.13931

John B Conway. 1994. *Functions of one complex variable I.* Springer-Verlag. doi:10.1007/978-1-4612-6313-5

Etienne Corman. 2024. Curvature-Driven Conformal Deformations. *ACM Trans. Graph.* 43, 4 (2024), 1–16. doi:10.1145/3658145

Keenan Crane. 2013. *Conformal geometry processing.* Ph.D. Dissertation. California Institute of Technology.

Mathieu Desbrun, Eva Kanso, and Yiying Tong. 2008. Discrete Differential Forms for Computational Modeling. In *Discrete Differential Geometry*, Alexander I. Bobenko, Peter Schröder, John M. Sullivan, and Günther M. Ziegler (Eds.). Oberwolfach Seminars, Vol. 38. Birkhäuser Verlag, 287–324.

Gerhard Dziuk and John E Hutchinson. 2006. Finite element approximations to surfaces of prescribed variable mean curvature. *Numer. Math.* 102, 4 (2006), 611–648. doi:10.1007/s00211-005-0649-7

Ilya Eckstein, Jean-Philippe Pons, Yiying Tong, C.-C. Jay Kuo, and Mathieu Desbrun. 2007. Generalized Surface Flows for Mesh Processing. In *Geometry Processing*, Alexander Belyaev and Michael Garland (Eds.). The Eurographics Association. doi:10.2312/SGP/SGP07/183-192

James Eells and Joseph H Sampson. 1964. Harmonic mappings of Riemannian manifolds. *Amer. J. Math.* 86, 1 (1964), 109–160. doi:10.2307/2373037

James Eells and John C Wood. 1976. Restrictions on harmonic maps of surfaces. *Topology* 15, 3 (1976), 263–266. doi:10.1016/0040-9383(76)90042-2

Michael S Floater, Kai Hormann, and Géza Kós. 2006. A general construction of barycentric coordinates over convex polygons. *Adv. Comput. Math.* 24, 1 (2006), 311–331. doi:10.1007/s10444-004-7611-6

Ilja Friedel, Peter Schröder, and Mathieu Desbrun. 2007. Unconstrained Spherical Parameterization. *J. Graph. Tools* 12, 1 (2007), 17–26. doi:10.1080/2151237X.2007.10129230

Mark Gillespie, Nicholas Sharp, and Keenan Crane. 2021. Integer coordinates for intrinsic geometry processing. *ACM Trans. Graph.* 40, 6 (2021). doi:10.1145/3478513.3480522

Eitan Grinspun, Anil Hirani, Mathieu Desbrun, and Peter Schröder. 2003. Discrete Shells. In *Proc. ACM/SIGGRAPH Conf.* 62–67.

Frédéric Hélein. 2001. *Constant mean curvature surfaces, harmonic maps and integrable systems.* Springer-Verlag. doi:10.1007/978-3-0348-8330-6

Tim Hoffmann. 1999. Discrete CMC Surfaces and Discrete Holomorphic Maps. *Discrete integrable geometry and physics* 16 (1999), 97.

Jürgen Jost. 1984. The Dirichlet problem for harmonic maps from a surface with boundary onto a 2-sphere with nonconstant boundary values. *J. Diff. Geom.* 19, 2 (1984), 393–401. doi:10.4310/jdg/1214438684

Wai Yeung Lam and Masashi Yasumoto. 2025. Discrete minimal surfaces: Old and New. *arXiv preprint arXiv:2510.23757* (2025).

Luc Lemaire. 1978. Applications harmoniques de surfaces riemanniennes. *J. Diff. Geom.* 13, 1 (1978), 51–78. doi:10.4310/jdg/1214434347

Dominic SP Leung. 2017. Reflection Principles for Smooth Harmonic Maps between Riemannian Manifolds and a Schwarz Reflection Principle for Harmonic and Holomorphic Maps from a Class of Hermitian Symmetric Spaces. *arXiv preprint arXiv:1707.01117* (2017). doi:10.48550/arXiv.1707.01117

Richard MacNeal. 1949. *Solution of Partial Differential Equations by means of Electrical Networks.* Ph. D. Dissertation. Caltech.

Antonin Monteil, Rémy Rodiac, and Jean Van Schaftingen. 2021. Ginzburg–Landau relaxation for harmonic maps on planar domains into a general compact vacuum manifold. *Arch. Ration. Mech. Anal.* 242, 2 (2021), 875–935. doi:10.1007/s00205-021-01695-8

John Neuberger. 2010. *Sobolev gradients and differential equations.* doi:10.1007/978-3-642-04041-2

Bernd Oberknapp and Konrad Polthier. 1997. An algorithm for discrete constant mean curvature surfaces. In *Visualization and Mathematics.* 141–161. doi:10.1007/978-3-642-59195-2_10

Frei Otto. 1967. Pneumatic Structures. In *Tensile Structures.* MIT Press.

Frei Otto and Bodo Rasch. 1995. *Finding form: towards an architecture of the minimal.*

Hao Pan, Yi-King Choi, Yang Liu, Wenchao Hu, Qiang Du, Konrad Polthier, Caiming Zhang, and Wenping Wang. 2012. Robust modeling of constant mean curvature surfaces. *ACM Trans. Graph.* 31, 4 (2012), 1–11. doi:10.1145/2185520.2335436

Davide Pellis, Martin Kilian, Helmut Pottmann, and Mark Pauly. 2021. Computational design of Weingarten surfaces. *ACM Trans. Graph.* 40, 4 (2021), 1–11. doi:10.1145/3450626.3459939

Davide Pellis, Hui Wang, Martin Kilian, Florian Rist, Helmut Pottmann, and Christian Müller. 2020. Principal symmetric meshes. *ACM Trans. Graph.* 39, 4 (2020), 127–1. doi:10.1145/3386569.3392446

Ulrich Pinkall and Konrad Polthier. 1993. Computing discrete minimal surfaces and their conjugates. *Experiment. Math.* 2, 1 (1993), 15–36. doi:10.1080/10586458.1993.10504266

Joseph Plateau. 1873. *Statique expérimentale et théorique des liquides soumis aux seules forces moléculaires.* Vol. 2. Gauthier-Villars.

Konrad Polthier and Wayne Rossman. 2002. Discrete constant mean curvature surfaces and their index. 549 (2002), 47–77. doi:10.1515/crll.2002.066

C Rogers and WK Schief. 2003. On the equilibrium of shell membranes under normal loading. Hidden integrability. *Proc. R. Soc. Lond. A* 459, 2038 (2003), 2449–2462. doi:10.1098/rspa.2003.1135

Ernst A Ruh and Jaak Vilms. 1970. The tension field of the Gauss map. *Trans. Amer. Math. Soc.* 149, 2 (1970), 569–573. doi:10.1090/s0002-9947-1970-0259768-5

Jonathan Sacks and Karen Uhlenbeck. 1981. The existence of minimal immersions of 2-spheres. *Ann. Math.* 113, 1 (1981), 1–24. doi:10.2307/1971131

Eike Schling. 2018. *Repetitive Structures.* Ph.D. Dissertation. TU Munich.

Nicholas Sharp, Yousuf Soliman, and Keenan Crane. 2019. Navigating Intrinsic Triangulations. *ACM Trans. Graph.* 38, 4 (2019). doi:10.1145/3306346.3322979

Jeffrey David Smith. 2003. *Three applications of optimization in computer graphics.* Ph.D. Dissertation. Carnegie Mellon University.

Yousuf Soliman, Albert Chern, Olga Diamanti, Felix Knöppel, Ulrich Pinkall, and Peter Schröder. 2021. Constrained Willmore surfaces. *ACM Trans. Graph.* 40, 4 (2021), 1–17. doi:10.1145/3450626.3459759

Rasmus Tamstorf and Eitan Grinspun. 2013. Discrete bending forces and their Jacobians. *Graphical Models* 75, 6 (2013), 362–370. doi:10.1016/j.gmod.2013.07.001

Xavier Tellier, Cyril Douthe, Olivier Baverel, and Laurent Hauswirth. 2023. Designing funicular grids with planar quads using isotropic Linear-Weingarten surfaces. *International Journal of Solids and Structures* 264 (2023), 112028. doi:10.1016/j.ijsolstr.2022.112028

Xavier Tellier, Laurent Hauswirth, Cyril Douthe, and Olivier Baverel. 2018. Discrete CMC surfaces for doubly-curved building envelopes. In *Adv. Architectur. Geom.* 166–193.

Stephanie Wang and Albert Chern. 2021. Computing Minimal Surfaces with Differential Forms. *ACM Trans. Graph.* 40, 4 (2021), 113:1–113:14. doi:10.1145/3450626.3459781

Max Wardetzky, Saurabh Mathur, Felix Kälberer, and Eitan Grinspun. 2007. Discrete Laplace operators: no free lunch. *Comp. Graph. Forum* 33 (2007), 37. doi:10.1145/1508044.1508063

Karl Weierstraß. 1866. *Untersuchungen über die Flächen, deren mittlere Krümmung überall gleich Null ist.*

A Möbius Geometric Discretization

A more robust alternative to the dual Dirichlet energy using inverse cotangent weights is motivated by the following relationship between a smooth immersion $f\colon M \to \mathbb{R}^3$ and its Gauß map $N\colon M \to \mathbb{S}^2$:

$$\mathcal{E}(N) = 2\mathcal{W}(f) + 2\pi\chi(M). \tag{18}$$

Here, the Willmore energy is $\mathcal{W}(f) = \int_M (H^2 - K)dA_f$ and the Dirichlet energy is $\mathcal{E}(N) = \frac{1}{2}\int_M \langle dN \wedge *dN\rangle$. In other words, the Dirichlet energy of N equals, up to a topological constant, the Willmore energy. Recall that the Willmore energy can be discretized following [Bobenko 2005] using the triangle circumcircle intersection angles β_{ij}:

$$\mathcal{W}(\mathrm{f}) \coloneqq \sum_{i\in\mathsf{V}} \mathcal{W}_i, \qquad \mathcal{W}_i \coloneqq \tfrac{1}{2}\Big(\sum_{ij} \beta_{ij} - 2\pi\Big).$$

In what follows we use the algebra of quaternions $\mathbb{H}$, identifying $\mathbb{R}^3$ with the purely imaginary quaternions. Using the quaternionic cross ratio, the circumcircle intersection angle β_{ij} can be expressed as:

$$\mathrm{e}_{il}\mathrm{e}_{lj}\mathrm{e}_{jk}\mathrm{e}_{ki} = -\cos\beta_{ij} + \sin\beta_{ij}\mathrm{n}^i_{ij},$$

where $\mathrm{e}_{ij} \coloneqq \mathrm{d}\mathrm{f}_{ij}/|\mathrm{d}\mathrm{f}_{ij}|$ are normalized edge vectors and n^i_{ij} the normal to their circumsphere at i. Computing

$$\mathrm{e}_{il}\mathrm{e}_{lj} = \cos\theta^{ji}_l - \sin\theta^{ji}_l \mathrm{N}_{jil},$$
$$\mathrm{e}_{jk}\mathrm{e}_{ki} = \cos\theta^{ij}_k - \sin\theta^{ij}_k \mathrm{N}_{ijk},$$

and looking only at the real part of the quaternionic cross ratio

$$-\cos\beta_{ij} = \cos\theta^{ij}_k\cos\theta^{ji}_l - \sin\theta^{ij}_k\sin\theta^{ji}_l\langle \mathrm{N}_{ijk}, \mathrm{N}_{jil}\rangle. \tag{19}$$

Relaxing the condition that N is the discrete Gauß map of an immersion, we are led to consider the function $\alpha \mapsto \beta_{ij}(\alpha)$ defined by Equation 19. To discretize the relationship in Equation 18, we consider the energy around an edge $ij \in \mathsf{E}$ defined by

$$\epsilon^{\mathrm{m\ddot{o}b}}_{ij}(\alpha) \coloneqq 2(\beta_{ij}(\cos\alpha) + \theta^{ij}_k + \theta^{ji}_l - \pi). \tag{20}$$

Its derivative is given by

$$\tfrac{1}{\sin\alpha}\tfrac{d}{d\alpha}\epsilon^{\mathrm{m\ddot{o}b}}_{ij}(\alpha) = \tfrac{2\sin\theta^{ij}_k\sin\theta^{ji}_l}{\sin\beta_{ij}(\alpha)}. \tag{21}$$

This is an even function and is monotone increasing for $\alpha \in [0,\pi]$. The monotonicity implies that $\epsilon^{\mathrm{m\ddot{o}b}}_{ij}(\alpha)$ is always non-negative[5], and the factor and constant shift are chosen so that:

Proposition A.1. *If $\theta^{ij}_k + \theta^{ji}_l < \pi$ then Equation 20 approximates the dual Dirichlet energy up to second order around the bending angle $\alpha = 0$:*

$$\epsilon^{m\ddot{o}b}_{ij}(\alpha) = \tfrac{1}{2}w^*_{ij}\alpha^2 + o(\alpha^2).$$

Proof. In the case $\alpha = 0$, we have that

$$\epsilon^{\mathrm{m\ddot{o}b}}_{ij}(0) = -\arccos(\cos(\theta^{ij}_k + \theta^{ji}_l)) + \theta^{ij}_k + \theta^{ji}_l = 0$$

since $\theta^{ij}_k + \theta^{ji}_l < \pi$. With $\epsilon^{\mathrm{m\ddot{o}b}}_{ij}$ an even function, we have $(\epsilon^{\mathrm{m\ddot{o}b}}_{ij})'(0) = 0$. To compute the second order coefficient, differentiate the function

$$F(\alpha) \coloneqq \cos\left(\theta^{ij}_k + \theta^{ji}_l - \tfrac{1}{2}\epsilon^{\mathrm{m\ddot{o}b}}_{ij}(\alpha)\right)$$

[5] for non-Delaunay edges ij, we have that $\epsilon^{\mathrm{m\ddot{o}b}}_{ij}(0) = 2(\theta^{ij}_k + \theta^{ji}_l) - \pi \geq 0$

twice at $\alpha = 0$ to find

$$\tfrac{1}{2}(\epsilon_{ij}^{\text{möb}})''(0) = \frac{\sin\theta_k^{ij}\sin\theta_l^{ji}}{\sin(\theta_k^{ij}+\theta_l^{ji})} = \tfrac{1}{2}w_{ij}^*. \qquad \square$$

This result (and its proof) is closely related to [Bobenko 2005, Proposition 11]. As anticipated, this discretization satisfies a discrete version of Equation 18:

Proposition A.2. *If* M *is closed,* $\frac{1}{2}\mathcal{E}_{\text{möb}}(\mathsf{N}) = \mathcal{W}(\mathsf{f}) + \pi\chi(\mathsf{M})$.

Proof. By the discrete Gauss-Bonnet theorem

$$\sum_{ij\in\mathsf{E}}(\theta_k^{ij}+\theta_l^{ji}) = \sum_{i\in\mathsf{V}}\sum_{ijk}\theta_{jk} = 2\pi(|\mathsf{V}| - \chi(\mathsf{M})),$$

from which the claim follows

$$\begin{aligned}\tfrac{1}{2}\mathcal{E}_{\text{möb}}(\mathsf{N}) &= \sum_{ij\in\mathsf{E}}(\beta_{ij}+\theta_k^{ij}+\theta_l^{ji}-\pi)\\ &= \Big(\sum_{ij\in\mathsf{E}}\beta_{ij}\Big) - \pi|\mathsf{V}| + \pi\chi(\mathsf{M}) = \mathcal{W}(\mathsf{f}) + \pi\chi(\mathsf{M}). \qquad \square\end{aligned}$$

A.1 Evaluation

To evaluate the Möbius geometric discretization of the Dirichlet energy, we consider the following experiment in Figure 20: given (1) a sequence of triangulated spheres with increasingly poor aspect ratio, we (2) sample the identity vector field on the vertices of the dual mesh, and (3) minimize the discrete Dirichlet energy using the dual energies $\mathcal{E}_{\text{cot}}$ and $\mathcal{E}_{\text{möb}}$. The negative edge weights of the non-Delaunay triangulations render the Dirichlet energy unstable when using the inverse cotangent weights, while the Möbius geometric discretization remains well-behaved. The discrete harmonic maps computed by minimizing $\mathcal{E}_{\text{möb}}$ still exhibit some dependency on the triangulation, as evidenced by the anisotropy compared to the ground truth (*i.e.*, the identity map).

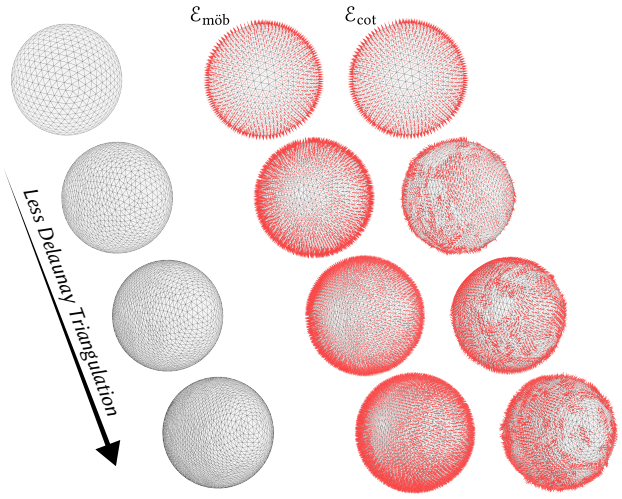

Fig. 20. **Recovering the Identity.** The identity map on $\mathbb{S}^2$ is harmonic. For less than perfect discretizations, minimizing Dirichlet energy based on inverse cotangent weights ($\mathcal{E}_{\text{cot}}$) fails to recover the identity map (*right*). The more robust $\mathcal{E}_{\text{möb}}$ produces a more reliable discrete approximation (*middle*).

B Newton Iterations

Introducing Lagrange multipliers $\Lambda \in \Omega^0(\mathsf{M};\mathbb{R})$ and using the unconstrained gradient 2-form of the energy $\operatorname{grad}\mathcal{E}(\mathsf{N}) \in \Omega^2(\mathsf{M}^*;\mathbb{R}^3)$ given by

$$\operatorname{grad}\mathcal{E}(\mathsf{N})_i = \sum_{ij}\frac{\epsilon'_{ij}(\alpha_{ij})}{\sin\alpha_{ij}}(\mathsf{N}_i - \mathsf{N}_j),$$

the first-order optimality conditions are a system of $4|\mathsf{V}|$ equations

$$\operatorname{grad}\mathcal{E}(\mathsf{N})_i + \Lambda_i\mathsf{N}_i = 0, \tag{22}$$

$$\tfrac{1}{2}(1 - \|\mathsf{N}_i\|^2) = 0, \tag{23}$$

one for each $i \in \mathsf{V}$. The first equation is an equivalent formulation of Equation 14. The Newton method updates $\delta\mathsf{N}$ and $\delta\Lambda$ are obtained by solving the sparse linear system

$$\begin{bmatrix}\operatorname{Hess}\mathcal{E} & \mathsf{X}^\top\\ \mathsf{X} & 0\end{bmatrix}\begin{bmatrix}\delta\mathsf{N}\\ \delta\Lambda\end{bmatrix} = -\begin{pmatrix}\operatorname{grad}\mathcal{E}(\mathsf{N}) + \Lambda\mathsf{N}\\ \frac{1}{2}(1-\|\mathsf{N}\|^2)\end{pmatrix},$$

where the multiplication $\Lambda\mathsf{N}$ and the length $\|\mathsf{N}\|$ are both understood componentwise, $\operatorname{Hess}\mathcal{E} \in \mathbb{R}^{3|\mathsf{V}|\times 3|\mathsf{V}|}$ is the Hessian of the discrete energy, and $\mathsf{X} \in \mathbb{R}^{|\mathsf{V}|\times 3|\mathsf{V}|}$ the Jacobian matrix of the unit norm constraint. X is a block $|\mathsf{V}| \times |\mathsf{V}|$ matrix consisting of (1×3) blocks $\mathsf{X}_{i,i} = \mathsf{N}_i^\top$. For the cotangent discretization of the Dirichlet energy $\operatorname{Hess}\mathcal{E}$ is the cotangent Laplacian.

C Poisson Integration

A closed one-form $\tau \in \Omega^1(M;\mathbb{R})$ on a simply connected domain M has an integral $g\colon M \to \mathbb{R}$ satisfying $dg = \tau$. The integral can be computed by solving a Poisson equation with suitable Neumann boundary conditions. The existence of the integral implies that g is the unique global minimizer of the quadratic functional

$$E(h) = \tfrac{1}{2}\|dh - \tau\|^2_{L^2(M)}.$$

By integration by parts, g satisfies

$$\mathring{E} = \int_M \langle d*dg - d*\tau, \mathring{g}\rangle - \int_{\partial M}\langle *(dg-\tau), \mathring{g}\rangle = 0$$

for all variations $\mathring{g}$. In particular, the Poisson equation that g satisfies by minimizing E over all possible functions is

$$\begin{cases} d*dg = d*\tau & \text{in } M,\\ \frac{\partial g}{\partial \nu} = \tau(\nu) & \text{on } \partial M.\end{cases}$$

In the discrete setting, we simply solve the matrix system

$$\mathsf{L}\mathsf{g} = \mathsf{d}_1^\top *_1 \tau,$$

with no modifications of the system along the boundary. This discretizes the natural boundary conditions above obtained by minimizing the energy globally.

D Harmonic Maps to $\mathbb{S}^2$

Since we reduce the computation of CMC surfaces to the computation of harmonic maps into $\mathbb{S}^2$, we review some of the relevant mathematical theory regarding the existence of harmonic maps into the two-sphere. While there exists a unique harmonic map in every homotopy class of maps from a Riemann surface M into a target space of non-positive curvature [Lemaire 1978], this does not hold when the target space is $\mathbb{S}^2$ [Eells and Wood 1976]. For example, if M is a torus there exists no such harmonic map of degree one. When

M is embedded in $\mathbb{R}^3$, by the Poincaré-Hopf theorem, the degree of its Gauß map is equal to $\frac{1}{2}\chi(M)$, and we expect that unless the homotopy class of maps under consideration agrees with this degree constraint there does not exist any harmonic map.

The harmonic map heat flow for maps into $\mathbb{S}^2$ also exhibits additional complications. For instance, Sacks and Uhlenbeck [1981] showed that the only way for the limit of a minimizing sequence to leave its homotopy class is by having a sphere "bubble off." On the other hand, we have the following positive result due to Jost [1984], which ensures that we can always find some constant mean curvature surface if we only work on a surface with boundary.

Theorem D.1. *Let M be a compact Riemann surface with non-empty boundary. For every non-constant Dirichlet boundary data $N|_{\partial M}\colon \partial M \to \mathbb{S}^2$ that admits a continuous extension to M with finite Dirichlet energy, there exist at least two harmonic extensions which minimize the energy in their respective homotopy classes.*

E Balanced Gauß Maps

Imposing a center of mass constraint on N is justified by noting that without such a constraint trivial solutions result from otherwise unconstrained optimization (see Section 5.3.4). Here we develop a suitable constraint on N in steps:

Theorem E.1. *Let M be a compact Riemann surface and $\tilde{M}$ its universal cover. Let $N\colon M \to \mathbb{S}^2$ be a non-constant and harmonic map which is not also conformal. Let $f\colon \tilde{M} \to \mathbb{R}^3$ be a CMC-$\frac{1}{2}$ surface with*

$$df = dN + N \times *dN.$$

Then

$$\int_M N\, dA = 0,$$

where dA is the area form induced by f.

Proof. Computing

$$d(f \times dN) = df \wedge dN = H\, df \wedge df = N\, dA.$$

Therefore, by Stokes' theorem

$$\int_M N\, dA = \int_M d(f \times dN) = \int_B f \times dN,$$

where B is a fundamental polygon in $\tilde{M}$ of M. Since N is defined on M the integral of dN along any edge of the fundamental polygon is zero. It then follows by the Riemann bilinear relations that

$$\int_B f \times dN = 0. \qquad \square$$

While the induced area form dA is only defined in the presence of f and when N is harmonic, we can equivalently express the constraint that N is balanced in a way that makes no reference to f. We first express the area form of f entirely through N:

$$\begin{aligned} N\, dA &= \frac{1}{2}(dN + N \times *dN) \wedge (dN + N \times *dN) \\ &= dN \wedge dN - N\,\langle dN \wedge *dN\rangle = d(N \times dN) + N\,\mu, \end{aligned}$$

where $\mu = \langle dN \wedge *dN\rangle$ is the Dirichlet energy density. It then follows from Theorem E.1 that

$$\int_M N\,\mu = 0. \tag{24}$$

A discrete analog of this theorem also holds. Since N is a unit vector $\mu_i := \langle (\mathrm{d} *_{\mathcal{E}} \mathrm{d}\mathsf{N})_i, \mathsf{N}_i\rangle$, and therefore, by integrating the discrete Euler-Lagrange equation (Equation 14) we obtain:

Theorem E.2. *Let $\mathsf{N}\colon \mathsf{V} \to \mathbb{S}^2$ be a critical point of $\mathcal{E}$. Then*

$$\sum_{i \in \mathsf{V}} \mathsf{N}_i \mu_i = 0$$

(*cf.*, Equation 24).

F Differentiating Through the Harmonic Extension

To compute the minimizers of the surface approximation functional from Section 5.2, we introduce the reduced energy $\tilde{\mathcal{F}}(N_0) = \mathcal{F}(N_0, \Phi(N_0))$ which depends on computing a discrete harmonic extension $\Phi(N_0)$. To compute its gradient we need to solve a linear system, which we describe explicitly for the vertex normal based discretization of harmonicity on a triangle mesh, and only minor modifications are needed to compute the gradient in the general case. Let us introduce the constraint mapping

$$c(\mathsf{N}_0, \mathsf{N}) = \begin{pmatrix} \mathsf{N}|_{V_\partial} - \mathsf{N}_0 \\ \mathsf{N} \times \mathsf{L}\mathsf{N} \end{pmatrix}$$

so that $\Phi(\mathsf{N}_0)$ is implicitly defined via the equation $c(\mathsf{N}_0, \Phi(\mathsf{N}_0)) = 0$. Using the chain rule

$$d\tilde{\mathcal{F}}_{\mathsf{N}_0}(\mathring{\mathsf{N}}_0) = \frac{\partial \mathcal{F}}{\partial \mathsf{N}_0}(\mathsf{N}_0, \Phi(\mathsf{N}_0))\mathring{\mathsf{N}}_0 + \frac{\partial \mathcal{F}}{\partial \mathsf{N}}(\mathsf{N}_0, \Phi(\mathsf{N}_0))(d\Phi_{\mathsf{N}_0}(\mathring{\mathsf{N}}_0)),$$

where $d\Phi_{\mathsf{N}_0}(\mathring{\mathsf{N}}_0)$ is given by

$$d\Phi_{\mathsf{N}_0}(\mathring{\mathsf{N}}_0) = -\left(\frac{\partial c}{\partial \mathsf{N}}(\mathsf{N}_0, \Phi(\mathsf{N}_0))\right)^{-1} \frac{\partial c}{\partial \mathsf{N}_0}(\mathsf{N}_0, \Phi(\mathsf{N}_0))\mathring{\mathsf{N}}_0.$$

It then follows that the differential of the reduced functional can be computed by solving a linearization of the discrete harmonic map equation

$$\begin{aligned} d\tilde{\mathcal{F}}_{\mathsf{N}_0} = \frac{\partial \mathcal{F}}{\partial \mathsf{N}_0}(\mathsf{N}_0, \Phi(\mathsf{N}_0)) \\ - \frac{\partial c}{\partial \mathsf{N}_0}(\mathsf{N}_0, \Phi(\mathsf{N}_0))^*\left(\frac{\partial c}{\partial \mathsf{N}}(\mathsf{N}_0, \Phi(\mathsf{N}_0))^*\right)^{-1} \frac{\partial \mathcal{F}}{\partial \mathsf{N}}(\mathsf{N}_0, \Phi(\mathsf{N}_0)). \end{aligned}$$

Explicitly,

$$\frac{\partial c}{\partial \mathsf{N}_0}(\mathsf{N}_0, \mathsf{N}) = \begin{matrix} \mathsf{V}_\partial \\ \mathsf{V}_I \end{matrix}\begin{bmatrix} -\mathrm{id} \\ 0 \end{bmatrix} \in \mathbb{R}^{3|\mathsf{V}| \times 3|\mathsf{V}_\partial|}$$

and

$$\frac{\partial c}{\partial \mathsf{N}}(\mathsf{N}_0, \mathsf{N}) = \begin{matrix} \mathsf{V}_\partial \\ \mathsf{V}_I \end{matrix}\begin{bmatrix} \mathsf{I} \\ \mathsf{A} \end{bmatrix} \in \mathbb{R}^{3|\mathsf{V}| \times 3|\mathsf{V}|},$$

where $\mathsf{I} \in \mathbb{R}^{3|\mathsf{V}_\partial| \times 3|\mathsf{V}|}$ defined by $\mathsf{I}_{ii} = 1$ for all $i \in \mathsf{V}_\partial$, and where for every vertex $i \in \mathsf{V}_I$ and every incident edge ij the matrix $\mathsf{A} \in \mathbb{R}^{3|\mathsf{V}_I| \times 3|\mathsf{V}|}$ is defined by

$$\mathsf{A}_{ii} := -[(\mathsf{L}\mathsf{N})_i]_\times, \quad \mathsf{A}_{ij} := [w_{ij}\mathsf{N}_i]_\times$$

G CMC Surfaces Touching a Plane

Let M be a simply connected Riemann surface and $\sigma\colon M \to M$ an antiholomorphic involution. Suppose that the fixedpoint set of σ is connected and separates M into two connected and simply connected components $\hat{M}$ and $\tilde{M}$, so

$$M = \hat{M} \cup \tilde{M}, \qquad \partial\hat{M} = \partial\tilde{M}.$$

Let $\hat{N}\colon \hat{M} \to \mathbb{S}^2$ be a harmonic map that sends $\partial\hat{M}$ to a constant point $\mathbf{a} \in \mathbb{S}^2$. Let R denote rotation by 180° around $\mathbf{a}$, so

$$R\mathbf{p} = 2\langle \mathbf{a}, \mathbf{p}\rangle \mathbf{a} - \mathbf{p}.$$

Then, by the Schwarz reflection principle as it applies to harmonic maps [Leung 2017, Theorem 4.1], we can extend $\hat{N}$ to a harmonic map

$$N\colon M \to \mathbb{S}^2$$
$$N = \begin{cases} \hat{N} & \text{on } \hat{M} \\ R\hat{N} \circ \sigma & \text{on } \tilde{M} \end{cases}$$

Let $g\colon M \to \mathbb{R}^3$ be such that

$$dg = N \times *dN, \qquad \langle \mathbf{a}, g\rangle = 0 \quad \text{on } \partial\hat{M}$$

and let $f_\pm = g \pm N$ be the corresponding CMC surfaces. Then we claim that

$$g = -Rg \circ \sigma$$

and

$$f_+ = -Rf_- \circ \sigma$$
$$f_- = -Rf_+ \circ \sigma.$$

To see this, we work in coordinates x, y near $\partial\hat{M}$ such that

$$*dx = dy \qquad *dy = -dx$$

and

$$x \circ \sigma = x \qquad y \circ \sigma = -y.$$

Then

$$\begin{aligned} dg &= N \times *dN = N \times (N_x\, dy \;-\; N_y\, dx) \\ &= (RN \circ \sigma) \times (RN_x \circ \sigma\, dy \;+\; RN_y \circ \sigma\, dx) \\ &= -(RN \circ \sigma) \times R\sigma^*(N_x\, dy - N_y\, dx) \\ &= -R\,\sigma^*(N \times *dN) = -R\,\sigma^* dg. \end{aligned}$$

So

$$g = -Rg \circ \sigma + \mathbf{v}$$

for some translation vector $\mathbf{v}$ and by our assumptions on g we have

$$-Rg(x, 0) \circ \sigma = g(x, 0),$$

which means $\mathbf{v} = 0$. The equations for f_+ and f_- follow immediately. Therefore, we have shown:

Theorem G.1. *If a $K \equiv 1$ surface g touches a plane along its boundary, it can be analytically continued as a $K \equiv 1$ surface across that plane by reflection in the plane.*

The same holds for the corresponding CMC surfaces f_+ and f_-. One only has to switch after reflection from f_+ to a translated version of its parallel surface f_- and vice versa.